OXFORD

Human Molecular Genetics, 2018, Vol. 27, No. 13 2290–2305

doi: 10.1093/hmg/ddy134
Advance Access Publication Date: 16 April 2018
Original Article

ORIGINAL ARTICLE

Elevated dual specificity protein phosphatase 4 in cardiomyopathy caused by lamin A/C gene mutation is primarily ERK1/2-dependent and its depletion improves cardiac function and survival

Jason C. Choi[1,*], Wei Wu[2,3], Elizabeth Phillips[1], Robin Plevin[4], Fusako Sera[2], Shunichi Homma[2] and Howard J. Worman[2,3,*]

[1]Department of Medicine, Center for Translational Medicine, Thomas Jefferson University, Philadelphia, PA 19107, USA, [2]Department of Medicine, [3]Department of Pathology and Cell Biology, Vagelos College of Physicians and Surgeons, Columbia University, New York, NY 10032, USA and [4]Strathclyde Institute of Pharmacy and Biomedical Sciences, University of Strathclyde, Glasgow G4 0RE, UK

*To whom correspondence should be addressed at: Department of Medicine, Center for Translational Medicine, Thomas Jefferson University, 1020 Locust Street JAH 236, Philadelphia, PA 19107, USA. Tel: +1 2155035685; Fax: 12155035731; Email: jason.x.choi@jefferson.edu (J.C.C.); Department of Medicine, College of Physicians and Surgeons, Columbia University, 630W 168th Street P&S 10-509, New York, NY 10032, USA. Tel: +1 2123051306; Fax: 12123420509; Email: hjw14@columbia.edu (H.J.W.)

Abstract

Mutations in the lamin A/C gene (*LMNA*) encoding the nuclear intermediate filament proteins lamins A and C cause a group of tissue-selective diseases, the most common of which is dilated cardiomyopathy (herein referred to as *LMNA* cardiomyopathy) with variable skeletal muscle involvement. We previously showed that cardiomyocyte-specific overexpression of dual specificity protein phosphatase 4 (DUSP4) is involved in the pathogenesis of *LMNA* cardiomyopathy. However, how mutations in *LMNA* activate *Dusp4* expression and whether it is necessary for the development of *LMNA* cardiomyopathy are currently unknown. We now show that female $Lmna^{H222P/H222P}$ mice, a model for *LMNA* cardiomyopathy, have increased *Dusp4* expression and hyperactivation of extracellular signal-regulated kinase (ERK) 1/2 with delayed kinetics relative to male mice, consistent with the sex-dependent delay in the onset and progression of disease. Mechanistically, we show that the H222P amino acid substitution in lamin A enhances its binding to ERK1/2 and increases sequestration at the nuclear envelope. Finally, we show that genetic deletion of *Dusp4* has beneficial effects on heart function and prolongs survival in $Lmna^{H222P/H222P}$ mice. These results further establish *Dusp4* as a key contributor to the pathogenesis of *LMNA* cardiomyopathy and a potential target for drug therapy.

Introduction

Mutations in the *LMNA* gene, which encodes lamins A and C (lamin A/C), cause a diverse group of diseases termed laminopathies. Despite its expression in most differentiated mammalian somatic cells, specific mutations in *LMNA* lead to tissue-selective diseases affecting striated muscle, adipose, or peripheral nerve as well as multi-system disorders with features of accelerated aging, such as Hutchinson–Gilford progeria syndrome (1). The most prevalent laminopathy is dilated cardiomyopathy (*LMNA* cardiomyopathy, OMIM #115200) with variable skeletal

Received: January 22, 2018. **Revised:** March 24, 2018. **Accepted:** April 9, 2018

muscle involvement, which includes autosomal Emery–Dreifuss muscular dystrophy and limb-girdle muscular dystrophy type 1B (2–5). *LMNA* cardiomyopathy, which may account for ~8% of familial cardiomyopathies, is characterized by early-onset conduction defects, ventricular dilatation, impaired contractility, and cardiac fibrosis, almost always progressing to congestive heart failure if not preceded by sudden death from cardiac dysrhythmia (6–11). Current therapeutic interventions involve implantable pacemakers and defibrillators as well as drugs commonly used to treat the symptoms of congestive heart failure such as angiotensin pathway inhibitors, aldosterone antagonists, diuretics, and beta-adrenergic blockers. While these therapies can prolong patient survival, they are targeted more at mitigating the complications and secondary features of the disease rather than the underlying pathogenic mechanisms.

Lamin A/C are intermediate filament proteins that constitute a major component of the nuclear lamina, a proteinaceous meshwork lining the inner nuclear membrane of metazoan cells (12). Although lamin A/C are widely accepted to provide structural support to the nucleus and maintain chromatin structure, more recent evidence demonstrates a dynamic role in regulating gene expression. For example, through epigenetic mechanisms, lamin A/C regulate gene expression programs necessary for tissue differentiation during development (13,14). Additionally, lamin A/C have been shown to act as a molecular scaffold that modulates cell signaling within the nuclear interior. The proteins directly interact with mitogen-activated protein (MAP) kinase extracellular signal-regulated kinase (ERK) 1/2 and its downstream transcription factor c-Fos, facilitating c-Fos phosphorylation at the nuclear lamina (15,16). Consistent with the regulatory role of lamin A/C in ERK1/2 signaling, ERK1/2 phosphorylation (which is indicative of its activation) is enhanced in hearts of human subjects with *LMNA* cardiomyopathy and in the *Lmna*$^{H222P/H222P}$ murine model (17,18). *Lmna*$^{H222P/H222P}$ mice recapitulate the cardiac pathology observed in human subjects, with male mice developing the disease with faster kinetics relative to female mice (19). Notably, the reduction of ERK1/2 signaling in these mice through genetic or pharmacological means achieves salutary effects on the heart as well as a prolongation of survival (18,20–22).

We have previously implicated the *Dusp4* gene encoding nuclear-resident dual specificity protein phosphatase 4 (DUSP4), which belongs to a superfamily of type I cysteine-based phosphatases that target MAP kinases, in the development of *LMNA* cardiomyopathy (23). We showed that *Dusp4* is overexpressed specifically in hearts of male *Lmna*$^{H222P/H222P}$ mice prior to detectable signs of cardiomyopathy and its expression is concomitant with activated protein kinase B (AKT)-mammalian target of rapamycin complex 1 (mTORC1) signaling and impaired autophagy (23,24). Moreover, transgenic mice with cardiac-specific overexpression of *Dusp4* exhibit molecular changes and heart defects analogous to those observed in the *Lmna*$^{H222P/H222P}$ mice, indicating that *Dusp4* overexpression is sufficient for the development of cardiomyopathy similar to that caused by *Lmna* mutations (23).

Early studies demonstrated that exposure of cells to fetal calf serum enhanced DUSP4 expression in an ERK1/2-dependent manner and its overexpression inhibited ERK1/2-dependent gene transcription (25–27). Based on these initial observations, as well as subsequent studies showing DUSP4-mediated dephosphorylation of additional members of the MAP kinase pathway, the primary function of this phosphatase was hypothesized to establish feedback inhibition of MAP kinase signaling (28–30). More recent studies have demonstrated diverse cellular inputs in addition to ERK1/2 signaling can stimulate *Dusp4* transcription (31–37). DUSP4 has also been shown to have other molecular functions besides MAP kinase dephosphorylation (38,39).

Pharmacological inhibition of ERK1/2 suppresses *Dusp4* expression in hearts from *Lmna*$^{H222P/H222P}$ mice and *in vitro* cell culture models (23). Although this suggests that ERK1/2 signaling is a predominant driver of DUSP4 expression in the heart in *LMNA* cardiomyopathy, confirmatory studies independent of pharmacological inhibitors are lacking. It is also unknown whether cardiomyopathy-causing *Lmna* mutations have a more direct effect on transcriptional activation as a result of epigenetic dysregulation on the *Dusp4* locus. Lastly, it is unknown whether DUSP4 protein overexpression, while shown to be sufficient, is required for the full phenotypic development of *LMNA* cardiomyopathy. In this study, we further establish DUSP4 as a mediator of *LMNA* cardiomyopathy pathogenesis by assessing the kinetics of its expression in hearts of female *Lmna*$^{H222P/H222P}$ mice that develop cardiac disease later than male mice. Using cellular models expressing disease-causing lamin A variants, we also present data suggestive of the molecular mechanisms that may underlie enhanced cardiac *Dusp4* expression in *Lmna*$^{H222P/H222P}$ mouse hearts. Lastly, we devise a model in which *Dusp4* is deleted from mice on the *Lmna*$^{H222P/H222P}$ background and show that DUSP4 depletion mitigates cardiomyopathy.

Results

Enhanced *Dusp4* expression in ventricular tissue of female *Lmna*$^{H222P/H222P}$ mice correlates with increases in markers of heart failure and fibrosis.

Female *Lmna*$^{H222P/H222P}$ mice develop dilated cardiomyopathy but with delayed kinetics relative to male mice (19). We previously reported enhanced ventricular *Dusp4* expression in male *Lmna*$^{H222P/H222P}$ mice starting as early as 4 weeks of age (23). We have also noted delayed kinetics of *Dusp4* expression in hearts of female *Lmna*$^{H222P/H222P}$ mice relative to males (23) but these initial observations were not fully explored. We therefore screened for the expression of 11 *Dusp* mRNAs in hearts of 20-week-old female *Lmna*$^{H222P/H222P}$ mice using quantitative real-time PCR (qPCR) (Fig. 1A). Similar to observations in male mice, we observed a specific statistically significant increase in *Dusp4* mRNA expression (~8-fold) in hearts of 20-week-old female *Lmna*$^{H222P/H222P}$ mice relative to *Lmna*$^{+/+}$ counterparts (Fig. 1A). The increased *Dusp4* expression was limited to cardiac and skeletal muscle (Fig. 1B). It was detectable at 20 weeks of age but not at 10 weeks of age, which is 6 weeks later than increased *Dusp4* expression is detected in hearts of male *Lmna*$^{H222P/H222P}$ mice (23) (Fig. 1C). To determine whether the increased *Dusp4* expression accompanied hyperactivated ERK1/2 and AKT signaling, as previously demonstrated in the hearts of male *Lmna*$^{H222P/H222P}$ mice (17,24), we assessed the expression of activated (phosphorylated) forms of these two signaling molecules. Consistent with the kinetics of DUSP4 expression, we observed increased levels of activated ERK1/2 and AKT, albeit with some animal to animal variability, in hearts of female *Lmna*$^{H222P/H222P}$ mice at 20 and 30 weeks of age but not at 10 weeks (Fig. 1D).

To determine if *Dusp4* expression coincided with expression of markers of heart failure, we examined the expression kinetics of natriuretic factors encoded by *Nppa* and *Nppb*, which are expressed as a consequence of left ventricular dilatation.

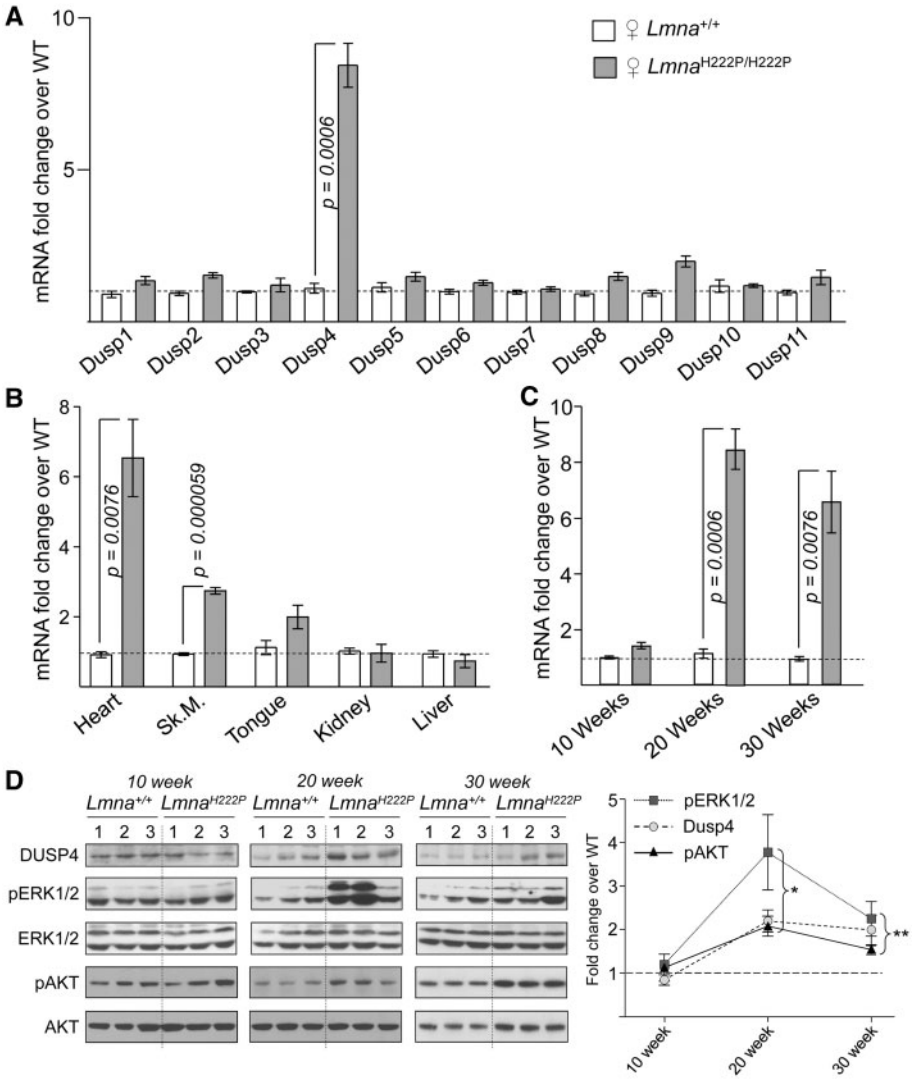

Figure 1. DUSP4 expression is enhanced in the ventricular tissue of female *Lmna*$^{H222P/H222P}$ mice. (**A**) qPCR analysis of *Dusp1*-*Dusp11* mRNA in hearts of 20-week-old female *Lmna*$^{H222P/H222P}$ mice compared to *Lmna*$^{+/+}$ (WT) mice. Values are means ± S.E.; $n = 3$ for each genotype. (**B**) qPCR analysis of *Dusp4* mRNA in hearts of 10-, 20-, and 30-week-old female *Lmna*$^{H222P/H222P}$ and *Lmna*$^{+/+}$ mice; $n = 3$. (**C**) qPCR analysis of *Dusp4* mRNA in indicated tissues from 30-week-old female *Lmna*$^{+/+}$ and *Lmna*$^{H222P/H222P}$ mice. 'SK.M.' denotes skeletal muscle (quadriceps); $n = 3$. (**D**) Western-blot analyses (left panel) of DUSP4, phospho-ERK1/2 (pERK1/2), total ERK1/2 (ERK1/2), phospho-serine 473 AKT (pAKT), and total AKT (AKT) in hearts of 10- to 30-week-old female *Lmna*$^{+/+}$ and *Lmna*$^{H222P/H222P}$ (*Lmna*^{H222P}) mice. Values are means ± S.E.; $n = 3$. Numbers on top of blots denote individual heart samples. Right panel shows quantification of pERK1/2, DUSP4, and pAKT in hearts of female *Lmna*$^{H222P/H222P}$ mice normalized to total ERK1/2 and AKT, respectively, and presented as fold-change over WT. Values are means ± S.E.; $n = 3$. Single (*$P < 0.05$) and double asterisks (**$P < 0.01$) represent *P*-values of normalized pERK1/2, DUSP4, and pAKT quantification relative to WT controls at 20 and 30 weeks of age, respectively.

Similar to *Dusp4* expression, *Nppa* and *Nppb* mRNA expression in hearts of female *Lmna*$^{H222P/H222P}$ mice was detected at 20 weeks of age and was further increased at 30 weeks (Fig. 2A). The increase in *Nppa* mRNA expression led to an increase in expression of the encoded atrial natriuretic protein (Fig. 2B). In addition, we measured mRNA levels of several collagen isoforms to assess for fibrotic responses. The level of type I collagen mRNA (*Col1a2*), which is only expressed by cardiac fibroblasts in the heart (40,41), was significantly enhanced by 10 weeks of age, prior to other detectable cardiac abnormalities, and further increased at 20 and 30 weeks (Fig. 2C). In contrast, collagen type IV mRNA (*Col4a1*, *Col4a2*), which is expressed by both cardiac fibroblasts and cardiomyocytes (40,41), showed modest increases that reached statistical significance only at 30 weeks of age (Fig. 2C). These data demonstrated that in female *Lmna*$^{H222P/H222P}$ mice, enhanced cardiac *Dusp4* expression accompanied altered cell signaling and expression of markers of left ventricular dilatation. In contrast, male *Lmna*$^{H222P/H222P}$ have earlier onset of *Dusp4* expression and altered cell signaling.

Enhanced *Dusp4* expression resulting from *Lmna* mutation is primarily driven by ERK1/2 pathway

Pharmacological inhibition of ERK1/2 activity suppresses *Dusp4* expression in hearts of *Lmna*$^{H222P/H222P}$ mice and *in vitro* cell culture models (23). This suggests that ERK1/2 signaling is the primary driver of increased *Dusp4* expression in hearts with a cardiomyopathy-causing *Lmna* mutation. However, it is plausible that *Lmna* mutation directly impinges on *Dusp4* expression

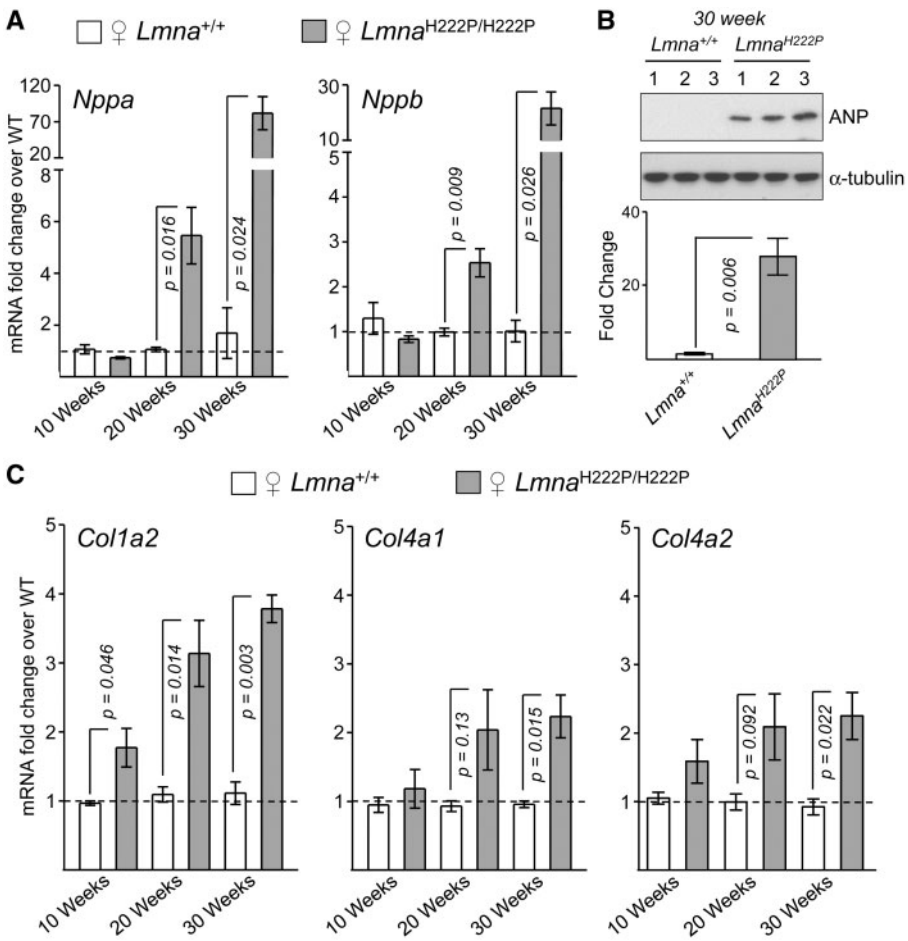

Figure 2. Expression of markers of left ventricular dilatation and ERK1/2 and AKT signal activation coincide with *Dusp4* expression in hearts of female *Lmna*$^{H222P/H222P}$ mice. (**A**) qPCR analysis of *Nppa* and *Nppb* mRNA in hearts of 10-, 20-, and 30-week-old female *Lmna*$^{+/+}$ (WT) and *Lmna*$^{H222P/H222P}$ mice; $n = 3$. (**B**) Western-blot analyses (top panel) of atrial natriuretic peptide (ANP) and α-tubulin in hearts of 30-week-old female *Lmna*$^{+/+}$ and *Lmna*$^{H222P/H222P}$ (*Lmna*^{H222P}) mice. Numbers on top of blots denote individual heart samples. Bottom panel shows quantification of ANP normalized to α-tubulin. Values are means ± S.E.; $n = 3$. (**C**) qPCR analysis of various collagen isoform mRNA in hearts of 10-, 20-, and 30-week-old female *Lmna*$^{+/+}$ and *Lmna*$^{H222P/H222P}$ mice. Values are means ± S.E.; $n = 3$.

independent of ERK1/2 pathway activation. Lamin A/C play a role in epigenetic regulation and pathogenic mutations in the *Lmna* gene cause alterations in epigenetic control (13,14,42). To determine whether the H222P lamin A/C expressed in *Lmna*$^{H222P/H222P}$ mice directly influence *Dusp4* expression by eliciting epigenetic changes at the *Dusp4* locus, we assessed its methylation and histone acetylation status upstream and downstream of the transcriptional start site.

To ascertain the likelihood of *Dusp4* methylation, we first performed *in silico* analysis for the presence of CpG islands within this locus. We analyzed a continuous stretch 2000 bp pairs encompassing the predicted transcriptional start site (TSS) within the *Dusp4* locus and found two prominent CpG islands that spanned the previously described promoter/enhancer regions (31,34–37) (Supplementary Material, Fig. S1A). To determine if specific CpG dinucleotides within the islands were methylated, we employed a strategy utilizing methylation-sensitive restriction enzyme digest analysis (Supplementary Material, Fig. S1B). We scanned the predicted CpG islands for the presence of both methylation sensitive and insensitive restriction endonuclease sites within close proximity to each other and found two such sites. The presence of DNA methylation was tested at these two sites in genomic DNA isolated from ventricular tissue of 8-week-old male *Lmna*$^{H222P/H222P}$ mice and compared to *Lmna*$^{+/+}$ counterparts. We found that both methylation sensitive and insensitive restriction enzymes were able to digest the genomic DNA and prevent amplicon generation using both semi-quantitative PCR (Supplementary Material, Fig. S1C–E) and quantitative PCR (Supplementary Material, Fig. S1F). This indicated that these specific sites within two prominent CpG islands within the *Dusp4* locus were not methylated. As a confirmatory experiment, we also cultured C2C12 cells stably expressing the H222P variant of FLAG-tagged lamin A, which overexpress *Dusp4* under glucose starvation (23), in the presence of the methylation inhibitor 5-aza-2′-deoxycytidine (5-AC). The presence of 5-AC (at 1 μM and 5 μM for 72 hr) did not further enhance *Dusp4* expression under either basal or glucose starved conditions (Supplementary Material, Fig. S2). Hence, our data indicated that enhanced *Dusp4* gene expression in hearts of *Lmna*$^{H222P/H222P}$ mice was not mediated by altered promoter/enhancer methylation.

Because DNA methylation did not appear to influence *Dusp4* expression, we performed chromatin immunoprecipitation (ChIP) analyses to determine if the H222P lamin A/C alter histone-3 acetylation (Ac-H3) at the *Dusp4* locus. Ac-H3-bound genomic DNA was immunoprecipitated from extracts of ventricular tissue of 8-week-old male *Lmna*$^{+/+}$ and *Lmna*$^{H222P/H222P}$ mice and probed for the enrichment of sequences that spanned

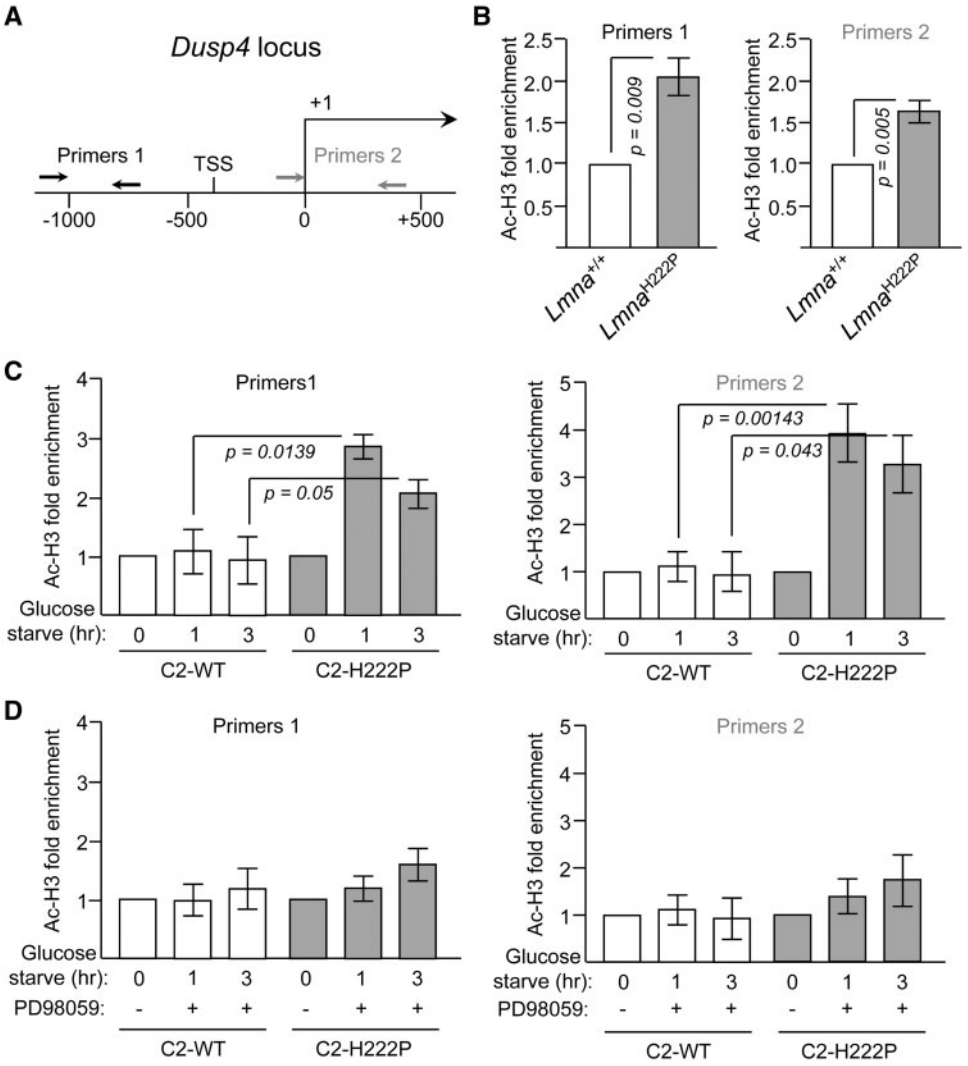

Figure 3. Histone 3-acetylation in the *Dusp4* promoter is enhanced in hearts of $Lmna^{H222P/H222P}$ mice and correlates with ERK1/2 signaling. (**A**) Schematic of the *Dusp4* locus and the locations of primer sets (black and gray arrows) used to amplify genomic DNA. 'TSS' and '+1' denote predicted transcription start site and the start codon, respectively. (**B**) ChIP analyses assessing enrichment of Ac-H3 in the *Dusp4* promoter of ventricular tissue isolated from 8-week-old male $Lmna^{+/+}$ and $Lmna^{H222P/H222P}$ ($Lmna^{H222P}$) mice; $n = 3$ for both primer sets 1 and 2. (**C**) ChIP analyses assessing enrichment of Ac-H3 in the *Dusp4* promoter of C2C12 myoblasts stably expressing WT (C2-WT) or H222P lamin A (C2-H222P) subjected to glucose starvation; $n = 3$. (**D**) ChIP analyses assessing enrichment of Ac-H3 in the *Dusp4* promoter of C2-WT or C2-H222P subjected to glucose starvation after 1 hr pretreatment with PD98058; $n = 3$. All values presented in this figure are means ± S.E. relative to WT, which was normalized to 1. The *P*-values are provided for pairwise comparisons that were statistically significant ($P < 0.05$).

the *Dusp4* transcriptional start site (Fig. 3A). qPCR analyses using two separate primer sets revealed a statistically significant increase in Ac-H3 at the *Dusp4* locus (Fig. 3B). This enhancement in Ac-H3 could be a direct result of H222P lamin A/C expression or occur indirectly via the ERK1/2 pathway, which is activated in hearts of male $Lmna^{H222P/H222P}$ mice by 4 weeks of age (17,23). To address this issue, we performed ChIP assays on C2C12 cells stably expressing either FLAG-tagged wild-type (WT) or H222P lamin A. When subjected to glucose deprivation, these cells recapitulate the phospho-ERK1/2 and *Dusp4* expression profiles observed in heart tissue of $Lmna^{+/+}$ and $Lmna^{H222P/H222P}$ mice (23). Under basal conditions, we observed no difference in the levels of Ac-H3 at the *Dusp4* locus between C2C12 cells expressing WT or H222P lamin A; however, upon removal of glucose, we observed significant increases in Ac-H3 only in cells expressing H222P lamin A (Fig. 3C). Given the inducibility of Ac-H3 at the *Dusp4* locus upon glucose deprivation, we surmised that this induction is due to the preferential increase in phospho-ERK1/2 as previously shown in C2C12 cells expressing H222P lamin A (23). Pretreatment of C2C12 cells with PD98059, which blocks ERK1/2 activity by inhibiting the upstream activator MEK1/2, abolished Ac-H3 enhancement at the *Dusp4* locus induced by glucose deprivation (Fig 3D). These data suggested that Ac-H3 at the *Dusp4* locus in cells expressing H222P lamin A variant, is primarily mediated by ERK1/2 activation.

To reinforce our data indicating that ERK1/2 signaling is the primary driver of *Dusp4* expression without relying on pharmacological inhibitors, we assessed its expression in hearts of $Lmna^{H222P/H222P}$ mice that were interbred with $Mapk3^{-/-}$ (encoding ERK1) mice to remove the influence of ERK1 (21) (Fig. 4A). Depletion of ERK1 from $Lmna^{H222P/H222P}$ mice prolonged survival and improved left ventricular function, which was abrogated at

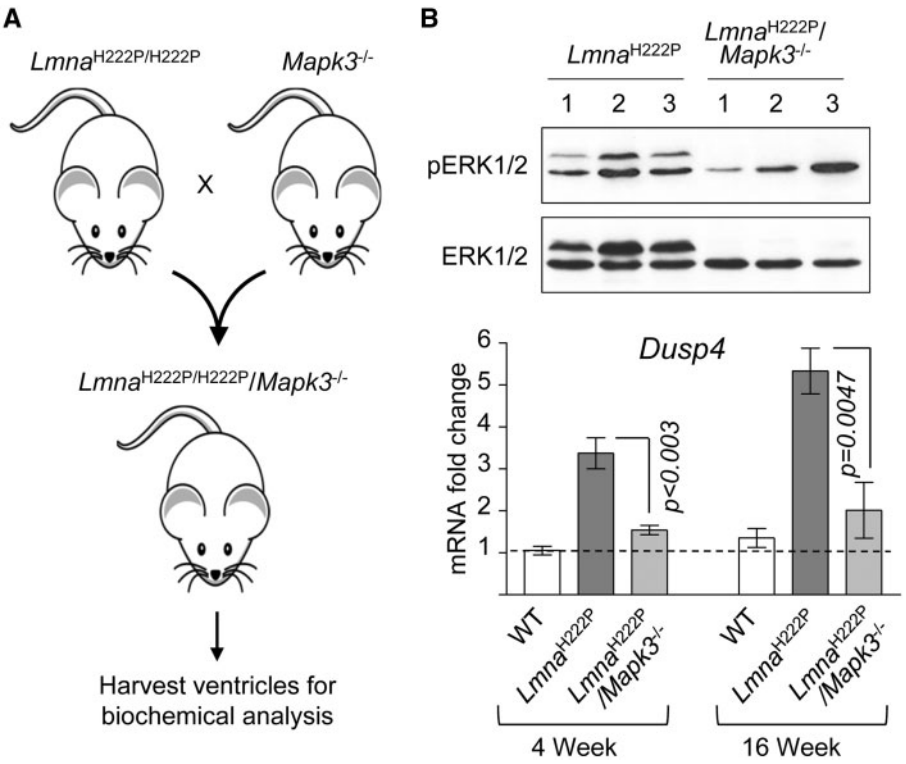

Figure 4. Genetic deletion of ERK1 impairs *Dusp4* expression. (**A**) Breeding strategy to delete *Mapk3* (ERK1) in *Lmna*$^{H222P/H222P}$ mice. (**B**) Western-blot analyses (top panel) of phospho-ERK1/2 and total ERK1/2 in hearts of 20-week-old male *Lmna*$^{H222P/H222P}$/*Mapk3*$^{+/+}$ (*Lmna*^{H222P}) and *Lmna*$^{H222P/H222P}$/*Mapk3*$^{-/-}$ mice. Numbers on top of blots denote individual heart samples. Bottom panel shows qPCR analysis of *Dusp4* mRNA in hearts of 4- and 16-week-old male *Lmna*$^{+/+}$/*Mapk3*$^{+/+}$ (WT), *Lmna*$^{H222P/H222P}$/*Mapk3*$^{+/+}$ (*Lmna*^{H222P}), and *Lmna*$^{H222P/H222P}$/*Mapk3*$^{-/-}$ double knockout (*Lmna*^{H222P}/*Mapk3*$^{-/-}$) mice. Values are means ± S.E.; $n = 3$ for each sample.

ages >20 weeks in male mice due to compensatory ERK2 hyperactivation (21). Expression of total and phosphorylated ERK1 were absent in hearts of *Lmna*$^{H222P/H222P}$/*Mapk3*$^{-/-}$ mice (Fig. 4B, top panel). This lack of ERK1 almost completely abolished *Dusp4* mRNA expression in hearts of *Lmna*$^{H222P/H222P}$/*Mapk3*$^{-/-}$ mice at both 4 and16 weeks of age relative to *Lmna*$^{H222P/H222P}$/*Mapk3*$^{+/+}$ mice despite the presence of phospho-ERK2 (Fig. 4B, bottom panel). To further confirm that *Dusp4* mRNA expression was primarily driven by ERK1/2-signaling, we also assessed the signaling status of p53, transforming growth factor-β (TGF-β), and the expression of E2F Transcription Factor 1, all of which have been shown to activate *Dusp4* transcription (32–35). We observed no significant changes in phosphorylated p53, phosphorylated Smad3 (induced by TGF-β signaling), or *E2f1* mRNA encoding E2F Transcription Factor 1 between hearts of 4-week-old *Lmna*$^{+/+}$ and *Lmna*$^{H222P/H222P}$ mice (Supplementary Material, Fig. S3). Although TGF-β signaling has been shown to be activated in hearts of male *Lmna*$^{H222P/H222P}$ mice at 20 weeks of age (19,43), we saw no evidence of its activation at 4 weeks, which is the earliest age at which *Dusp4* is overexpressed (23). These results demonstrated that enhanced ERK1/2 signaling underlies *Dusp4* overexpression in hearts of *Lmna*$^{H222P/H222P}$ mice.

H222P lamin A preferentially sequesters ERK1/2 at the nuclear lamina

Previous studies have demonstrated that lamin A/C can bind to phospho-ERK1/2 and that the resulting recruitment of these protein kinases to the nuclear lamina may facilitate the downstream propagation of mitogenic signaling (15,16). It is unknown if pathogenic lamin A variants impinge on the ability to bind to ERK1/2. We therefore investigated the effects of the cardiomyopathy-associated H222P lamin A variant and a disease control variant on binding to ERK1/2.

Gonzalez *et al.* previously reported co-immunoprecipitation of phospho-ERK1/2 following pull-down of endogenous lamin A/C (15). However, our attempts using similar approaches with C2C12 cells stably expressing FLAG-tagged WT lamin A or variants with amino acid substitutions were unsuccessful. While we reliably co-immunoprecipitated ERK1/2 with lamin A, the levels were very low and inconsistent when comparing WT and variants of lamin A between experiments (data not shown). We surmised that this was due to the technical challenge inherent in extracting and solubilizing lamin A/C, an intermediate filament protein, from the nuclear lamina.

Traditionally, chaotropic agents such as high concentrations of urea or sodium dodecyl sulfate (SDS) have been used to extract and solubilize lamin A/C. Based on our attempts to immunoprecipitate both endogenous or overexpressed lamin A and its variants, we concluded that methods that effectively extract and solubilize the protein also destroy meaningful *in vivo* associations. To circumvent this technical hurdle, we pursued an alternative approach utilizing *in vitro* binding using immunoprecipitated lamin A (Fig. 5A). Plasmids encoding FLAG-tagged WT lamin A, H222P lamin A, or R482W lamin A (a variant causing Dunnigan-type familial partial lipodystrophy) were transiently transfected into 293T cells, which were then lysed in extraction buffer containing ionic detergents (0.1% SDS and 0.5% sodium deoxycholate) and sonicated. The overexpressed FLAG-tagged lamin A was then immunoprecipitated using M2 anti-FLAG affinity gel. The purified gel-lamin A complexes (acting as 'bait') were washed and incubated with whole

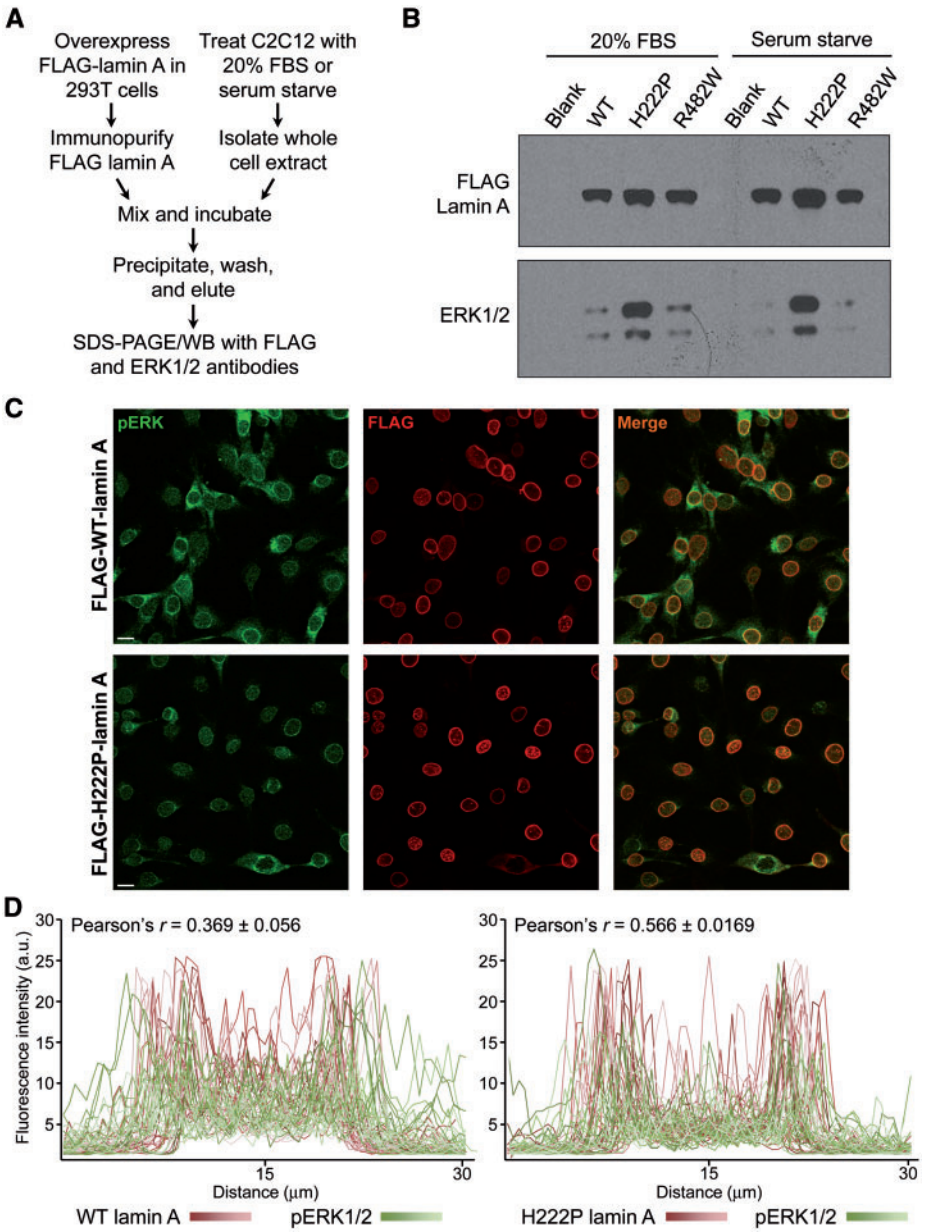

Figure 5. ERK1/2 preferentially binds to H222P lamin A and localizes to the nuclear envelope. (**A**) Experimental design of *in vitro* binding analysis between immunoprecipitated lamin A variants and ERK1/2. WB indicates western blot. (**B**) Autoradiograms showing western blots of immunoprecipitated WT and indicated lamin A variants incubated with whole cell extracts isolated from C2C12 cells subjected to either 20% fetal bovine serum or serum starvation. Blank indicates control samples in which blank expression vector was used to transfect 293T cells instead of lamin A expression vectors. Four independent experiments were performed with similar results. (**C**) Confocal micrographs of C2C12 cells stably expressing either FLAG-tagged WT or H222P lamin A stained with FLAG and phospho-ERK1/2 antibodies. Scale bar = 20 μm. (**D**) Fluorescence intensity profiles of WT lamin A, H222P lamin A, and phospho-ERK1/2 determined from line measurements along the cell length that bisect the nucleus in cells from panel 5C. Red shaded lines indicate WT or H222P lamin A and the green shaded phospho-ERK1/2 measured from 30 individual cells from two separate experiments. Pearson's *r* (means ± S.E.) was calculated from a total of 6 images per experimental group across 3 independent experiments.

extracts from C2C12 cells (source of ERK1/2 acting as 'prey'), which were prepared using a lysis buffer lacking ionic detergents (see Materials and Methods for details). The bait-prey complexes were pelleted/washed, eluted, and assessed for the presence of ERK1/2 using SDS–PAGE and western blotting. Whole cell extracts from C2C12 cells treated with either 20% fetal bovine serum or serum starved for 30 minutes were used to ascertain whether the phosphorylation status of ERK1/2 influenced its biding to lamin A. We also repeated the experiment using extracts from immortalized mouse embryonic fibroblasts lacking lamin A/C (iMEF$^{-/-}$) to remove potential confounding influence of the presence of endogenous WT lamin A/C in C2C12 cell extracts. Increased and reduced phospho-ERK1/2 levels following high serum treatment and serum starvation, respectively, were confirmed in aliquots of C2C12 and iMEF$^{-/-}$ extracts used as prey (Supplementary Material, Fig. S4A). We observed that, relative to WT and R482W lamin A, H222P lamin A co-precipitated with the greatest amount of total ERK1/2 from both C2C12 and iMEF$^{-/-}$ extracts (Fig. 5B and Supplementary Material, Fig. S4B). We observed no difference in lamin A

binding to ERK1/2 between 20% serum-treated and serum starved C2C12 and iMEF$^{-/-}$ extracts used as prey (Fig. 5B and Supplementary Material, Fig. S4B), suggesting that the phosphorylation status of ERK1/2 did not affect their binding to lamin A.

To ascertain the level of phospho-ERK1/2 from the total ERK1/2 that co-precipitated with lamin A, we performed western blot with anti-phospho-ERK1/2 antibodies. However, despite multiple attempts with several commercially available phospho-ERK1/2 antibodies, we were not able to detect phospho-ERK1/2. As an alternative strategy, we performed confocal microscopy on C2C12 cells stably expressing either FLAG-tagged WT or H222P lamin A. We previously showed that these cells expressed identical levels of the FLAG-tagged lamin A transgenes (23). We labeled fixed cells with phospho-ERK1/2 antibodies to assess its localization. Confocal micrographs showed that phospho-ERK1/2 were localized to the nuclear rim in cells expressing H222P lamin A to a greater degree than in those expressing the WT protein (Fig. 5C). Linear fluorescence intensity measurements across the nucleus along the length of the cell as well as Pearson's r analysis confirmed our initial observation of greater co-localization between phospho-ERK1/2 and H222P lamin A compared to WT lamin A (Fig. 5D). Similar results were obtained in C2C12 cells stably expressing non-FLAG-tagged WT lamin A, N195K (another point mutant variant associated with striated muscle disease) lamin A and H222P lamin A variants (Supplementary Material, Fig. S5), indicating that the FLAG tag did not alter lamin A-ERK1/2 binding characteristics. These results demonstrate that the H222P amino acid substitution in lamin A results in increased binding to total ERK1/2, relative to the WT or lipodystrophy-associated R482W variant, and, as a consequence, enhanced sequestration of phospho-ERK1/2 at the nuclear lamina.

Deletion of *Dusp4* in *Lmna*$^{H222P/H222P}$ mice has beneficial effects on cardiac function and prolongs survival

To test directly the hypothesis that *Dusp4* expression is a key contributor to the pathophysiology of cardiomyopathy, we crossbred *Lmna*$^{H222P/H222P}$ mice to *Dusp4*$^{-/-}$ mice (Fig. 6A). We confirmed the lack of DUSP4 protein expression in ventricular tissue extracts from the resulting interbred mice (Supplementary Material, Fig. S6). Depleting DUSP4 from male *Lmna*$^{H222P/H222P}$ mice (*Lmna*$^{H222P/H222P}$/*Dusp4*$^{-/-}$) significantly increased their medial survival (Fig. 6B). Echocardiography showed that prolonged survival correlated with improved cardiac parameters such as reduction in left ventricular end systolic diameter as well as increases in fractional shortening and ejection fraction (Fig. 6C and D). We also observed a subtle but significant decrease in fractional shortening in *Lmna*$^{+/+}$/*Dusp4*$^{-/-}$ mice relative to *Lmna*$^{+/+}$/*Dusp4*$^{+/+}$ controls, which has been reported previously (44).

We examined hematoxylin and eosin stained sections of left ventricles from 20-week-old *Lmna*$^{+/+}$/*Dusp4*$^{-/-}$ (control), *Lmna*$^{H222P/H222P}$/*Dusp4*$^{+/+}$, and *Lmna*$^{H222P/H222P}$/*Dusp4*$^{-/-}$ mice (Fig. 7A). Consistent with our recent report (22), we observed pronounced cytoplasmic vacuolation within cardiomyocytes of the papillary muscles accompanied by variations in myocyte size in hearts of *Lmna*$^{H222P/H222P}$/*Dusp4*$^{+/+}$ mice (Fig. 7A). These abnormalities were virtually absent in papillary muscles of *Lmna*$^{+/+}$/*Dusp4*$^{-/-}$ mice (Fig. 7A, left panel) and significantly reduced (~2-fold reduction) in *Lmna*$^{H222P/H222P}$/*Dusp4*$^{-/-}$ mice (Fig. 7A, right panel and Fig. 7B). Massson's trichrome staining to detect fibrosis revealed no significant differences between the genotypes (data not shown).

We previously showed that autophagic responses were blunted in hearts of mice overexpressing *Dusp4* due to aberrant activation of the AKT-mTORC1 pathway (23,24). Therefore, we assessed AKT-mTORC1 signaling by assessing the activation (phosphorylation) of AKT and mTOR (a central component of mTORC1) as well as markers of autophagy in *Lmna*$^{H222P/H222P}$/*Dusp4*$^{-/-}$ mice. Western-blot analyses of protein extracts isolated from ventricular tissue of *Lmna*$^{H222P/H222P}$/*Dusp4*$^{+/+}$ and *Lmna*$^{H222P/H222P}$/*Dusp4*$^{-/-}$ mice revealed significantly reduced AKT phosphorylation with the deletion of *Dusp4*; however, the reduction in mTOR phosphorylation did not attain statistical significance (Fig. 7C). To assess the impact of incomplete deactivation of mTOR on autophagy, we measured autophagic responses by detecting for increased levels of lipidated microtubule-associated protein-1 light chain 3 β (LC3B-II) from its non-lipidated form (LC3B-I) as an indirect measure of autophagosome formation (45,46) (Fig. 7C). We also measured the level of p62/SQSTM1 (p62), a LC3B-binding protein that is degraded following autophagosome fusion with lysosomes as an indirect measure of autophagic flux (Fig. 7C). Consistent with incomplete deactivation of mTOR, our results showed a trend toward autophagy activation but the change in levels of LC3B-II and p62 in hearts of *Lmna*$^{H222P/H222P}$/*Dusp4*$^{-/-}$ mice did not reach statistical significance (Fig. 7C). These results indicate that AKT and mTORC1 signaling may be decoupled in hearts of *Lmna*$^{H222P/H222P}$/*DUSP4*$^{-/-}$ mice. We did observe a statistically significant enhancement in phospho-ERK1/2 level, most likely due to the depletion of DUSP4 (Fig. 7C).

Discussion

Our results show that *Dusp4* contributes to the pathogenesis of *LMNA* cardiomyopathy. The delayed kinetics of cardiac *Dusp4* expression in female *Lmna*$^{H222P/H222P}$ mice relative to male counterparts coincided with the corresponding delay in the onset detectable heart dysfunction (19). A previous study found that androgen receptor accumulation in the nucleus of cardiomyocytes contributes to the sex-dependent differences observed in the *Lmna*$^{H222P/H222P}$ mice (47). This suggests a putative crosstalk mechanism between ERK1/2-Dusp4 and androgen receptor function. In support of this idea, a previous report demonstrated that testosterone induces cardiomyocyte hypertrophy through ERK1/2-dependent mTORC1 activation (48). Sex-dependent differences have also been reported in patients with *LMNA* cardiomyopathy. Men with the disease are more likely to succumb to malignant ventricular arrhythmia and end-stage heart failure (49,50). However, no differences are observed in the age of onset or the rate of disease progression to end-stage heart failure or death (49). It is unclear whether the sex differences in patients with *LMNA* cardiomyopathy are mediated by *LMNA*-specific mechanisms or due to better overall prognosis in women with heart failure (51,52).

We showed that the enhanced ERK1/2 signaling is predominantly responsible for the increased *Dusp4* expression in response to the H222P *Lmna* mutation. This is in contrast to other instances in which direct perturbations of genetic loci involving epigenetic mechanisms occur as a direct consequence of *Lmna* mutations (13,14,42). The increased Ac-H3 at the *Dusp4* locus was dependent on ERK1/2 signaling in C2C12 cell culture models expressing WT and H222P lamin A variants indicating that transcription promoting epigenetic changes occurs as a consequence of kinase activation. In addition, *Dusp4* expression was

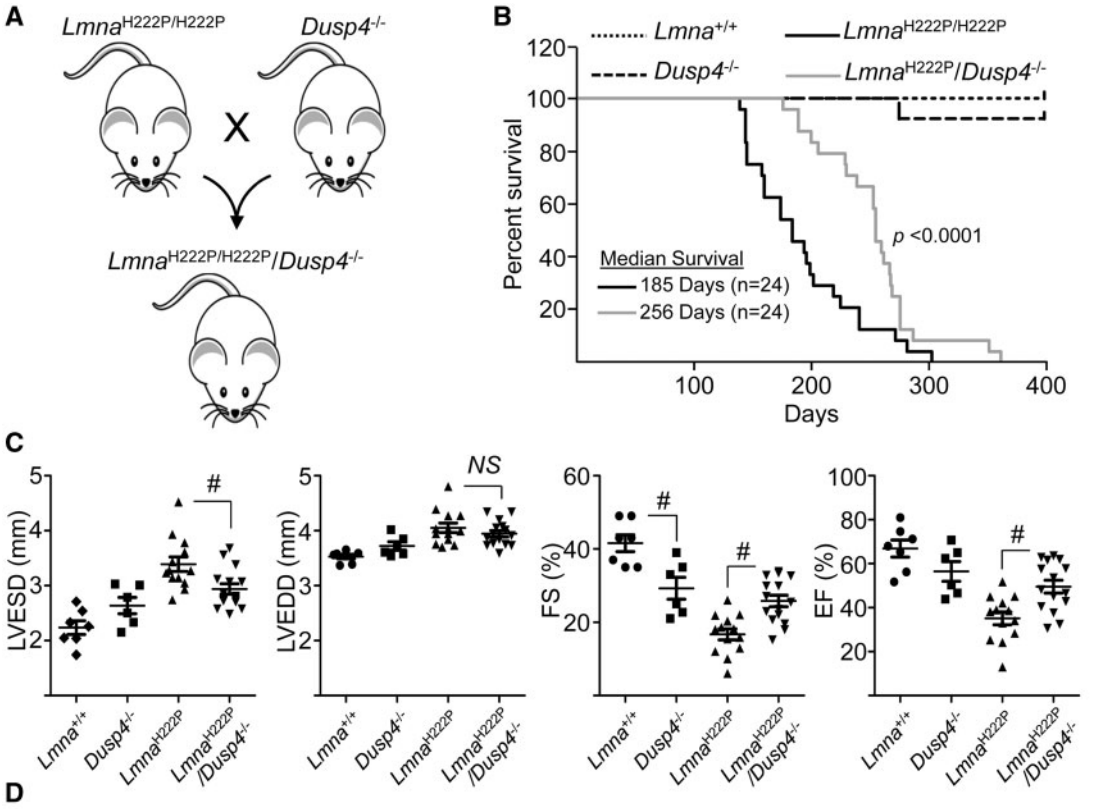

D

Genotype	HR/min (bpm)	LVESD (mm)	LVEDD (mm)	FS (%)	EF (%)
Lmna$^{+/+}$ (n=7)	500.4 ± 1.64	2.24 ± 0.123	3.53 ± 0.040	41.6 ± 2.3	66.8 ± 3.9
Dusp4$^{-/-}$ (n=6)	502.5 ± 0.95	2.64 ± 0.149	3.72 ± 0.076	29.3 ± 3.0	56.5 ± 4.5
Lmna$^{H222P/H222P}$ (n=13)	502.3 ± 0.73	3.39 ± 0.132	4.05 ± 0.086	16.7 ± 1.5	35.2 ± 2.9
Lmna$^{H222P/H222P}$ */Dusp4*$^{-/-}$ (n=15)	501.2 ± 0.73	2.94 ± 0.095	3.94 ± 0.058	25.8 ± 1.6	49.5 ± 2.9

Figure 6. Genetic deletion of *Dusp4* in *Lmna*$^{H222P/H222P}$ mice increases survival and cardiac performance parameters. (**A**) Breeding strategy to delete *Dusp4* in *Lmna*$^{H222P/H222P}$ mice. (**B**) Kaplan–Meier estimator plot of survival of *Lmna*$^{+/+}$/*Dusp4*$^{+/+}$ (*Lmna*$^{+/+}$), *Lmna*$^{+/+}$/*Dusp4*$^{-/-}$ (*Dusp4*$^{-/-}$), *Lmna*$^{H222P/H222P}$/*Dusp4*$^{+/+}$ (*Lmna*$^{H222P/H222P}$), and *Lmna*$^{H222P/H222P}$/*Dusp4*$^{-/-}$ (*Lmna*^{H222P}/*Dusp4*$^{-/-}$) mice. The *P*-value was derived using log-rank (Mantel–Cox) test. (**C**) Graphic representation of M-mode echocardiographic tracing measurements for left ventricular end systolic diameter (LVESD), left ventricular end diastolic diameter (LVEDD), fractional shortening (FS), and ejection fraction (EF) of hearts from *Lmna*$^{+/+}$/*Dusp4*$^{+/+}$ (*Lmna*$^{+/+}$), *Lmna*$^{+/+}$/*Dusp4*$^{-/-}$ (*Dusp4*$^{-/-}$), *Lmna*$^{H222P/H222P}$/*Dusp4*$^{+/+}$ (*Lmna*^{H222P}), and *Lmna*$^{H222P/H222P}$/*Dusp4*$^{-/-}$ (*Lmna*^{H222P}/*Dusp4*$^{-/-}$) mice ∼20 weeks of age. Values for individual mice are shown; horizontal lines indicate means and error bars are S.E. '#' indicates that the comparisons were statistically significant (95% confidence interval) as determined by one-way ANOVA with *post hoc* Tukey's multiple comparison test. *NS* denotes not significant. (**D**) Numerical values for heart rate (HR) indicated as beats per minute (bpm), LVESD, LVEDD, FS, and EF of hearts from *Lmna*$^{+/+}$/*Dusp4*$^{+/+}$ (*Lmna*$^{+/+}$), *Lmna*$^{+/+}$/*Dusp4*$^{-/-}$ (*Dusp4*$^{-/-}$), *Lmna*$^{H222P/H222P}$/*Dusp4*$^{+/+}$ (*Lmna*$^{H222P/H222P}$), and *Lmna*$^{H222P/H222P}$/*Dusp4*$^{-/-}$ mice at ∼20 weeks of age.

significantly reduced in hearts of *Lmna*$^{H222P/H222P}$ mice lacking ERK1 at both 4 and 16 weeks of age, further confirming that ERK1/2 signaling underlies *Dusp4* expression.

In addition to cardiomyopathy, *Lmna*$^{H222P/H222P}$ mice develop muscular dystrophy (19). We previously showed that quadriceps of 16-week-old male *Lmna*$^{H222P/H222P}$ mice also exhibit enhanced *Dusp4* expression albeit to a lesser degree relative to the heart (23). The current study demonstrates similar findings in quadriceps of female *Lmna*$^{H222P/H222P}$ mice. Elevated phospho-ERK1/2 levels have been observed in multiple skeletal muscle groups of *Lmna*$^{H222P/H222P}$ mice and systemic administration of small molecule inhibitors of MEK1/2 improves skeletal muscle pathology and limb grip strength (53). These studies collectively suggest that activation of ERK1/2 in skeletal muscle may be responsible for the enhanced *Dusp4* expression and underlie skeletal muscle pathogenesis.

Our results from *in vitro* models showed increased total ERK1/2 binding to the myopathy-associated lamin A H222P variant relative to the WT protein or the lipodystrophy-causing R482W variant. This enhanced binding did not appear to be influenced by ERK1/2 phosphorylation status, which is consistent with previously published observations (16). We also showed a corresponding increase in phospho-ERK1/2 localization at the nuclear lamina in H222P lamin A-expressing C2C12 cells. These results are consistent with the hypothesis that the H222P amino acid substitution in lamin A/C causes enhanced total ERK1/2 binding irrespective of phosphorylation status and, as a consequence, increased localization of phosphorylated

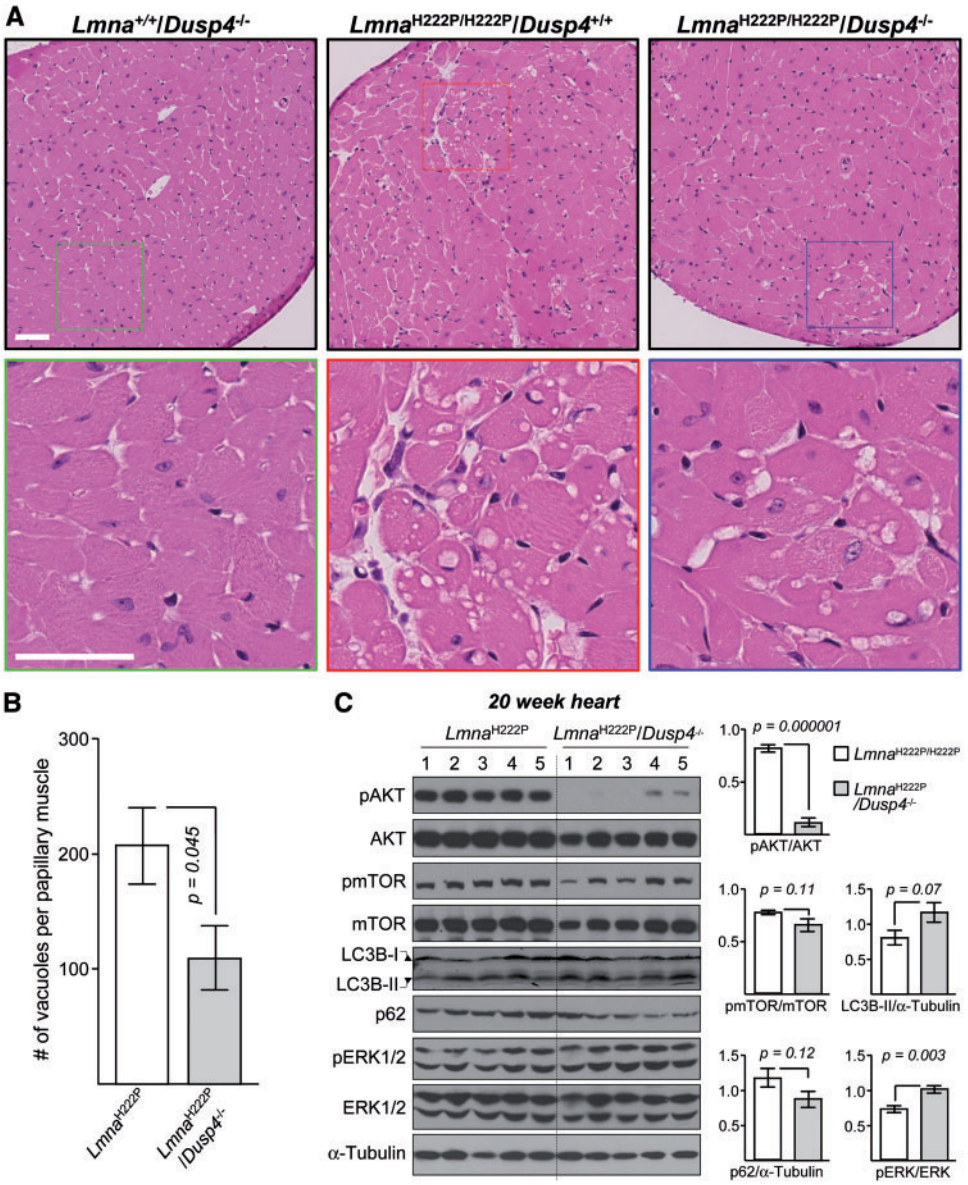

Figure 7. Papillary muscle myofiber structural aberrations in the *Lmna*$^{H222P/H222P}$ mice are reduced with genetic deletion of *Dusp4* with weak correlation with enhanced autophagy. (**A**) Photomicrographs of hematoxylin and eosin stained left ventricle sections from *Lmna*$^{+/+}$/*Dusp4*$^{-/-}$, *Lmna*$^{H222P/H222P}$/*Dusp4*$^{+/+}$, and *Lmna*$^{H222P/H222P}$/*Dusp4*$^{-/-}$ mice. The colored boxes in the top panels are shown at higher magnification in the lower panels. Scale bar = 50 μm. (**B**) Quantification of papillary muscle cytoplasmic vacuolation in *Lmna*$^{H222P/H222P}$/*Dusp4*$^{+/+}$ (*Lmna*^{H222P}) and *Lmna*$^{H222P/H222P}$/*Dusp4*$^{-/-}$ (*Lmna*^{H222P}/*Dusp4*$^{-/-}$) mice from a total area of 800 μm x 500 μm per papillary muscle; $n = 3$ for each genotype. The data are presented as number of vacuoles in the papillary muscle. Values are means ± S.E. (**C**) Western-blot analyses (left panel) of phospho-serine 473 AKT (pAKT), total AKT (AKT), phospho-mTOR, (pmTOR), total mTOR (mTOR), LC3B-I (non-lipidated), LC3B-II (lipidated), p62, phospho-ERK1/2 (pERK1/2), total ERK1/2 (ERK1/2), and α-tubulin in protein extracts from hearts of *Lmna*$^{H222P/H222P}$/*Dusp4*$^{+/+}$ (*Lmna*^{H222P}) and *Lmna*$^{H222P/H222P}$/*Dusp4*$^{-/-}$ (*Lmna*^{H222P}/*Dusp4*$^{-/-}$) mice. Numbers above each lane indicate an individual mouse. Right panel shows quantification analysis of the blots. Values are means ± S.E.; $n = 5$.

ERK1/2 at the nuclear lamina. Despite our data from *in vitro* binding and cell culture models, we acknowledge that the significance of the apparently enhanced binding affinity of the H222P lamin A variant to ERK1/2 remains uncertain in driving kinase hyper-activation in *LMNA* cardiomyopathy. First, it is difficult to explain how this altered binding affinity observed in the cultured cells we examined could lead to the observed selectivity of ERK1/2 hyperactivation in striated muscle in animals (17,23). Secondly, loss of lamin A/C in mice and haploinsufficiency in humans leads to cardiomyopathy (2,54). This would not lead to enhanced ERK1/2 binding to lamin A/C but could hypothetically alter the properties of the entire lamina, including B-type lamins, with regards to kinase sequestration.

Our data demonstrating ERK1/2 signaling as the predominant driver of Dusp4 expression coupled with its established function as a negative feedback inhibitor of ERK1/2 present an obvious conundrum: how are levels of both phosphorylated ERK1/2 and Dusp4 enhanced in the hearts of *Lmna*$^{H222P/H222P}$ mice? Furthermore, the original study linking ERK1/2 activation and *LMNA* cardiomyopathy demonstrated increased nuclear localization of phospho-ERK1/2 in hearts of *Lmna*$^{H222P/H222P}$ mice (17), which further contributes to the apparent paradox.

A hypothesis consistent with our observations is one in which the scaffolding function of the nuclear lamina is disrupted in a way that disrupts efficient binding between ERK1/2 and Dusp4, in a manner similar to the role of lamin A/C bridging the interaction between activated ERK1/2 and c-Fos (15,55). Moreover, it was recently shown that activated ERK1/2 catalyzes a phosphorylation reaction on the C-terminus of DUSP4 protein that increases its half-life (56,57). Therefore, the potential scaffolding role of the nuclear lamina facilitating the interaction of DUSP4 with ERK1/2 may be a critical regulatory point for ERK1/2 signal output. The disruption of this function by the expression of the H222P lamin A/C variant may facilitate the continued activation of ERK1/2 downstream effectors (one of which is DUSP4), while the newly expressed DUSP4 is unable to efficiently dephosphorylate ERK1/2. This hypothesis remains to be tested.

Arguably, the most significant finding of our current study is the salutary effects of *Dusp4* gene deletion in the *Lmna*$^{H222P/H222P}$ background. *Lmna*$^{H222P/H222P}$/*Dusp4*$^{-/-}$ mice displayed improved cardiac performance parameters, mainly due to the preservation of systolic dimensions, and this improvement was correlated with prolonged survival compared to *Lmna*$^{H222P/H222P}$/*Dusp4*$^{+/+}$ mice. Although male *Lmna*$^{H222P/H222P}$/*Dusp4*$^{+/+}$ mice develop significant cardiac fibrosis at 6 months of age (19), we observed minimal fibrosis in both *Lmna*$^{H222P/H222P}$/*Dusp4*$^{+/+}$ and *Lmna*$^{H222P/H222P}$/*Dusp4*$^{-/-}$ male mice at ~4.5 months of age, probably due to the earlier age at which the analysis was performed. We did observe abnormal myofibers, particularly in the papillary muscles in the *Lmna*$^{H222P/H222P}$/*Dusp4*$^{+/+}$ mice in the form of cytoplasmic vacuolation, and these abnormalities were significantly reduced in the *Lmna*$^{H222P/H222P}$/*Dusp4*$^{-/-}$ mice. These improvements were observed despite higher levels of phospho-ERK1/2 in hearts of *Lmna*$^{H222P/H222P}$/*Dusp4*$^{-/-}$ mice relative to *Lmna*$^{H222P/H222P}$/*Dusp4*$^{+/+}$ mice. We surmise the increased phospho-ERK1/2, despite the lack of DUSP4 expression, may undercut the salutary effects of *Dusp4* deletion. By extension, we hypothesize that activated ERK1/2 and overexpression of DUSP4 separately contribute to *LMNA* cardiomyopathy. Furthermore, the concurrent ERK1/2 activation and DUSP4 overexpression, which is the cardiac expression profile in the *Lmna*$^{H222P/H222P}$/*Dusp4*$^{+/+}$ mice, may be required for the full penetrance of the disease phenotype. We previously showed that transgenic mice overexpressing *Dusp4* specifically in cardiomyocytes displayed decreased phospho-ERK1/2 and increased DUSP4 expression in the heart and developed a subtler cardiac phenotype in the form of reduced systolic dimension compared to *Lmna*$^{H222P/H222P}$ mice (23). In this study, we present evidence of a subtle but significant reduction in left ventricular fractional shortening in hearts of 20-week-old *Lmna*$^{+/+}$/*Dusp4*$^{-/-}$ mice relative to *Lmna*$^{+/+}$/*Dusp4*$^{+/+}$ mice. Phospho-ERK1/2 levels were variable with only some samples showing slight increases (data not shown). This is consistent with a previous report studying *Lmna*$^{+/+}$/*Dusp4*$^{-/-}$ mice, although in the decreases in fractional shortening were observed later at 8 months of age (44). Additionally, *Lmna*$^{H222P/H222P}$/*Dusp4*$^{-/-}$ mice showed improved cardiac performance parameters relative to *Lmna*$^{H222P/H222P}$/*Dusp4*$^{+/+}$ mice, mainly due to the preservation of systolic dimensions, despite modestly increased phospho-ERK1/2 levels. These data collectively suggest that activated ERK1/2 and DUSP4 uniquely contribute to the pathogenesis of *LMNA* cardiomyopathy and that both could be targeted for effective therapy.

AKT-mTORC1 signaling is aberrantly activated in the hearts of *Lmna*$^{H222P/H222P}$ and mice lacking lamin A/C and its activation prevents cardiac induction of autophagy, which is thought to underlie the pathogenesis of cardiomyopathy (24,58). We also previously showed that enhanced cardiac expression of *Dusp4* causes aberrant AKT-mTORC1 activation (23). Although the levels of activated AKT (phosphorylation of S473) were significantly reduced in hearts of *Lmna*$^{H222P/H222P}$/*Dusp4*$^{-/-}$ mice relative to *Lmna*$^{H222P/H222P}$/*Dusp4*$^{+/+}$ mice, a corresponding reduction in mTOR activation and subsequent activation of autophagy were not statistically significant. These results suggest a decoupling between AKT and mTOR activation in the hearts of *Lmna*$^{H222P/H222P}$/*Dusp4*$^{-/-}$ mice. AKT activates mTORC1 through an intermediary termed tuberin sclerosis complex (TSC) composed of TSC1, TSC2, and Rheb (59). TSC2 is a GTPase activating protein targeting Rheb, a Ras family GTPase (59). Activated AKT catalyzes an inhibitory phosphorylation on multiple serine and threonine residues on TSC2, which reduces the Rheb GTPase activity, and increases the level of GTP-bound Rheb (60,61). The GTP-bound Rheb then directly binds and activates mTOR (62), leading to downstream effector functions of mTORC1 such as inhibition of autophagy (63). Notably, activated ERK1/2 can also catalyze an inhibitory phosphorylation on TSC2 at the unique serine 664 residue that results in mTOR activation (64). Given that DUSP4 is a feedback inhibitor of ERK1/2 signaling, the depletion of DUSP4 and the resulting increase in the level of activated ERK1/2 in the hearts of *Lmna*$^{H222P/H222P}$/*Dusp4*$^{-/-}$ mice may lead to an incomplete deactivation of mTOR despite AKT inactivation. Our results indicate that although the genetic deletion of *Dusp4* leads to improved survival and cardiac function, its full beneficial effect may be blunted by the incomplete deactivation of mTOR (and hence partial activation of autophagy) mediated by another process, such as enhancement of the ERK1/2-TSC2 pathway. Alternatively, it is plausible that AKT-dependent pathways may contribute more substantially to the deterioration of cardiac function and mortality than mTOR-mediated mechanisms in the development of *LMNA* cardiomyopathy. Although the AKT pathway is necessary for the beneficial effects of exercise-induced physiological hypertrophy (65), prolonged activation leads to cardiomyopathy whereas transient activation improves cardiac function (66,67).

From a therapeutic perspective, the development of pharmacological inhibitors targeting DUSP4 has trailed behind functional and structural discoveries. Part of the reason is due to the nature of DUSP4 structure as well as its biochemical functionality. The active sites of DUSPs are ~6 Å, which is shallower than those of protein tyrosine phosphatases at ~9 Å (68). The active site of DUSP4 is even shallower than other DUSPs (69), presenting a significant challenge in achieving specificity in inhibition with small molecules. Furthermore, DUSP4-mediated dephosphorylation is a first-order reaction requiring only direct binding to its target (68). Because ATP hydrolysis is dispensable for phosphatase-mediated dephosphorylation, DUSP4 lacks an ATP binding pocket commonly targeted by small molecule inhibitors, presenting an additional obstacle in the development of effective and specific drug development. An alternative strategy to inhibit DUSP4, as supported by our results, is to target ERK1/2 signaling. As stated earlier, activated ERK1/2 not only stimulate *Dusp4* transcription but also stabilize the protein by phosphorylating its C-terminus, leading to an increased half-life (56,57). Given our conclusion that ERK1/2 are dominant drivers of *Dusp4* expression in *LMNA* cardiomyopathy, as well as accumulating evidence showing that their blockade has therapeutic benefit in mouse models of *LMNA* cardiomyopathy (18,20–22,70), a treatment strategy targeting ERK1/2 (perhaps in combination with AKT inhibition) presents a superior therapeutic option than direct DUSP4 inhibition.

Materials and Methods

Mice

The Columbia University Medical Center Institutional Animal Care and Use Committee approved all protocols using animals and the investigators adhered to the NIH Guide for the Care and Use of Laboratory Animals. *Lmna*$^{H222P/H222P}$ mice (C57BL/6 genetic background) were obtained from Dr Gisèle Bonne (Institut de Myologie, Paris) and genotyped using tail biopsies as described (19). *Dusp4*$^{-/-}$ mice (C57BL/6 genetic background) genotyped as described (71). Heart tissue from intercrosses between *Lmna*$^{H222P/H222P}$ and *Mapk3*$^{-/-}$ mice (from Drs Gilles Pagès and Jacques Pouysségur—Université de Nice) were generated in mixed background (129 and C57BL/6) and genotyped as described (21,72). Genotyping was performed by PCR using genomic DNA isolated from tail clippings. Mice were fed a chow diet and housed in a disease-free barrier facility with 12/12 hr light/dark cycles.

Cells

Generation and characterization of C2C12 myoblasts stably expressing FLAG-tagged WT, H222P, and R482W lamin A as well as the non-FLAG-tagged versions of WT, N195K, and H222P lamin A have been described elsewhere (23). For FLAG-lamin A expressing cells, cDNAs from these cells were PCR amplified with primers corresponding to FLAG and mouse lamin A and the resultant amplicons were sequenced to confirm the correct WT and H222P lamin A variant expression. These cells as well as 293T cells, iMEF$^{-/-}$ [from *Lmna*$^{\Delta 8-11}$ mice (73), previously *Lmna*$^{-/-}$ mice (54)] and unmodified C2C12 cells were cultured in Dulbecco's modified Eagle's medium containing 10% fetal bovine serum (FBS). All C2C12 cells were subcultured prior to reaching ~80% cell confluency.

RNA isolation and qPCR

Total RNA was isolated using TRIzol and cDNAs generated from 1 μg primed with a 1:1 ratio of random hexameric primers and oligo dT using SuperScript Reverse Transcriptase II (Invitrogen). qPCR was performed on an ABI 7300 Real-Time PCR system (Applied Biosystems) using SYBR green (USB). qPCR primers for *Dusp1–11*, *Nppa*, *Nppb*, *Col1a2*, and *Hprt* have been described elsewhere (17,20,70,74). *Col4a1* (For—5′-ATGGCATTGTGGAGTG TCAA; Rev—5′-TGTCCAGGGAAACCAATCTC), *Col4a2* (For—5′-CA TCCGTCGGAGATGAAGAT; Rev—5′-CCTTTGTACCGTTGCATC CT), and *E2f1* (For—5′-AGGGTCCCTATGGAAGAGGA; Rev—5′-CAGGTCCCCAAAGTCACAGT) primers were generated using Primer3 (http://bioinfo.ut.ee/primer3-0.4.0/primer3/; date last accessed April 23, 2018). *Hprt* mRNA was assessed to ensure equal fidelity in enzymatic reactions and was used as internal control to normalize qPCR results. Fold-changes in gene expression were determined by the ΔΔCt method (75) and are presented as fold-change over WT controls.

Protein extraction and western-blot analysis

Hearts were excised from sacrificed mice and tissue homogenized in radioimmunoprecipitation assay (RIPA) buffer (Sigma–Aldrich) with protease inhibitor cocktail (Roche), 1 mM phenylmethylsulfonyl fluoride (Sigma–Aldrich), and 1 mM sodium vanadate. Following brief sonication (Dismembrator Model F60, Thermo Fisher Scientific), 15 to 30 μg of protein extract was loaded for SDS–PAGE. Antibodies against the following proteins were purchased from Cell Signaling Technology: phospho-AKT (Ser473 #4060), AKT (#4691), phospho-ERK1/2 (#9101), LC3B, (#2775), phospho-mTOR (Ser2448 #2971), mTOR (#2972), phospho-Smad3 (#9520), Smad2/3 (#3102), phospho-p53 (Ser15 #9284), and p53 (#2524). Antibodies against the following proteins were purchased from Santa Cruz Biotechnology: ERK1/2 (sc-94), DUSP4 (sc-1200), ANP (sc-20158), and α-tubulin (sc-12462-R). GAPDH antibodies were purchased from Ambion (#AM4300). Quantification of blots was performed with ImageJ (76), normalized to loading controls as indicated, and presented as arbitrary units or fold-change over untreated or WT controls.

Epigenetic analysis

In silico methylation analysis of murine *Dusp4* upstream promoter sequence of C57BL/6J reference sequence (NCBI—NC_000074.6) was performed using EMBOSS Cpgplot (http://www.ebi.ac.uk/Tools/seqstats/emboss_cpgplot/; date last accessed April 23, 2018). For methylation analysis using restriction enzymes, purified genomic DNA from hearts of *Lmna*$^{+/+}$ and *Lmna*$^{H222P/H222P}$ mice was digested overnight with restriction enzyme SphI (New England BioLabs), which cuts at sites −7067 and +6474 from the *Dusp4* start codon, generating an ~13.5 kb contiguous genomic sequence spanning the *Dusp4* predicted TSS (37). The digested DNA was aliquoted and subsequently cleaved by restriction enzyme digestion with ZraI, BsrBI, AhdI, or BlpI (New England BioLabs) followed by enzymatic reaction cleanup. Then, 50 ng of cleaved genomic DNA was amplified by PCR using the following primers: For 5′-GAAGACCTCCACACGGAGAG and Rev 5′-TTGCTAGCTAGGGCT GCTTC for ZraI site (−568 bp from start codon) and For 5′-CAGCTAGCTCCCCAGCTTAC and Rev 5′-GGCACCCACGTTTA CCTTTA for BsrBI site (+134 bp). *Hprt* (same primers used for RT-qPCR analysis) was assessed as the internal loading control. ChIP assay was performed using EZ-ChIP (Millipore) according to the manufacturer's instructions for C2C12 cells stably expressing FLAG-tagged WT and H222P lamin A. Glucose starvation and 20 μM PD98059 treatment of these cells were performed as described previously (23). Minor modifications were made for the heart tissue ChIP as established by Weinmann and Farnham (77). Briefly, ~80 mg of ventricular tissue was minced into small pieces (between 1–3 mm^3) and crosslinked with 1% formaldehyde in 800 μl of PBS (1 ml PBS per 100 mg of tissue) with protease inhibitor cocktail II (PI-II, provided by EZ-ChIP) for 15 minutes. Crosslinking was quenched by adding freshly prepared glycine to a final concentration of 0.125M and incubating at room temperature for 5 minutes. The crosslinked tissue pieces were pelleted, washed twice with ice cold PBS with PI-II, and homogenized in 1 ml of SDS lysis buffer + PI-II as indicated and provided by the manufacturer. Chromatin shearing (750–250 bp fragments) was achieved using a sonicator (Dismembrator Model F60) for a total of 4 minutes at 20 second intervals for C2C12 cells and 7 minutes for the heart tissue. Antibodies against Ac-H3 and isotype-matched control antibodies (both provided by the manufacturer) were used to immunoprecipitate Ac-H3 bound DNA and non-specific DNA, respectively. In addition, 1% of total sheared chromatin was collected and assessed as 'input' to ensure comparable levels of starting material. The purified DNA isolated from immunoprecipitated and input samples were subjected to qPCR using primers For 5′-CCCCCTCTGGGTTGTAAAGT and Rev 5′-GCTCGGGGACTTTGTGAAT for primer set 1 and For 5′-CAGCTAGCTCCCCAGCTTAC and Rev 5′-GGCACCCACGTTTACCT TTA for primer set 2.

Microscopy and histopathological analysis

Immunofluorescence staining was performed on stable methanol: acetone (3:1)-fixed C2C12 cells using standard protocols with anti-phospho-ERK1/2 (Cell Signaling Technology, #9101), anti-FLAG (for FLAG-tagged lamin A—clone M5, Sigma–Aldrich), and lamin A/C (for non-FLAG mutant variants—MANLAC1) antibodies. Confocal images were captured using a LSM 510 confocal laser scanning system (Carl Zeiss) in the Confocal and Specialized Microscopy Core at the Herbert Irving Comprehensive Cancer Center (Columbia University Medical Center). Fluorescence intensity profiles of lamin A (and its variant used in the study) and phospho-ERK1/2 were determined using the ImageJ software (76) using methods similar to those described by Gonzalez *et al.* (15). Linear fluorescence intensity of lamin A and phospho-ERK1/2 were measured from 30 individual cells from two separate experiments. Co-localization analyses of lamin A and phospho-ERK1/2 signals and the calculation of Pearson's *r* were performed using JACoP ImageJ plugin (78). Hemotoxylin and eosin staining of formaldehyde-fixed and paraffin-embedded heart was performed by Molecular Pathology Shared Resource in the Herbert Irving Comprehensive Cancer Center (Columbia University Medical Center). Stained slides were scanned with a Leica SCN400 auto brightfield whole slide digital scanning system and visualized using the Aperio ImageScope software (Leica Systems). The quantification of papillary muscle cytoplasmic vacuolation was performed at 20X magnification on 40 contiguous 100 μm^2 images (a total area of 800 μm x 500 μm) per papillary muscle in a blinded fashion by an investigator blind to mouse genotype. The data are presented as number of vacuoles in the papillary muscle within the 800 μm x 500 μm field analyzed.

Lamin A variant immunoprecipitation and *in vitro* binding analysis

293T cells were transiently transfected with expression vectors (pEGFP-C1, Invitrogen) containing cDNA sequences for either the WT, H222P, or R482W lamin A, in which the EGFP sequence was replaced by the FLAG sequence in the backbone vector. The vectors were confirmed by DNA sequencing. The transfected cells were lysed in RIPA buffer (Sigma–Aldrich) with PI and the FLAG-tagged lamin A and its point mutant variants were solubilized by sonication (Dismembrator Model F60) and immunoprecipitated using anti-FLAG M2 affinity agarose gel (Sigma–Aldrich). The precipitated agarose gel was washed twice with 1X RIPA buffer followed by another two washes with 0.5X RIPA buffer and stored for future use. C2C12 and iMEF$^{-/-}$ that were either serum starved or stimulated with 20% FBS were lysed in 1X Cell Lysis Buffer (Cell Signaling Technology), which lacks ionic detergents. The isolated cell extracts were added to the immunoprecipitated lamin A in equal volumes and the mixture was incubated overnight at 4°C rotating end-over-end. The protein complexes were washed twice in 0.5X Cell Lysis Buffer followed by two washes with 1X Cell Lysis Buffer. The protein complexes were eluted from the agarose gel by boiling in 2X Laemmli (79) buffer containing 5% β-mercaptoethanol and resolved by SDS–PAGE.

Transthoracic echocardiography and survival analysis

Lmna$^{+/+}$/*Dusp4*$^{+/+}$, *Lmna*$^{+/+}$/*Dusp4*$^{-/-}$, *Lmna*$^{H222P/H222P}$/*Dusp4*$^{+/+}$, and *Lmna*$^{H222P/H222P}$/*Dusp4*$^{-/-}$ mice were anesthetized with 1–2% isoflurane and placed on a heating pad (37°C) attached to an electrocardiographic monitor. Echocardiography was performed using Vevo 770 imaging system (VisualSonics) equipped with a 30 MHz transducer. Parameters were measured for at least three cardiac cycles. An echocardiographer blind to mouse genotype performed the examinations and interpreted the results. Survival analysis was performed until time of death or signs of significant distress requiring euthanasia. Specific signs of significant distress included 1) difficulty with normal ambulatory movement, 2) failure to eat or drink, 3) significant weight loss of >20%, 4) depression, 5) unkempt hair coat, and 6) significant respiratory distress. A staff veterinarian at the Institute of Comparative Medicine at Columbia University Medical Center, blind to mouse genotype, determined if euthanasia was required. Those requiring euthanasia were sacrificed according to the protocol of the Institute of Comparative Medicine consistent with American Veterinary Medical Association guidelines.

Statistical analysis

Graphpad (Prism Software) was used to perform statistical analyses. Statistical significance of binary variables from scanned western blots, qPCR results, and papillary muscle vacuole quantification were determined by a 2-tailed, unpaired Student's *t*-test with a value of $P < 0.05$ considered significant. Values with error bars shown in figures are means ± S.E.M. Sample sizes are indicated in the figure legends. Echocardiographic measurements comparing the four different genotypes were determined by one-way ANOVA with *post hoc* Tukey's multiple comparison test ($P < 0.05$ considered significant). Mouse survival was analyzed using the Kaplan–Meier estimator and the differences in median survival compared using a log-rank (Mantel–Cox) test with $P < 0.05$ considered to be statistically significant.

Supplementary Material

Supplementary Material is available at *HMG* online.

Acknowledgements

We thank Dr Gisèle Bonne (Institut de Myologie) for providing *Lmna*$^{H222P/H222P}$ mice, Drs Gilles Pagès and Jacques Pouysségur (Université de Nice) form providing *Mapk3*$^{-/-}$ mice and Dr Colin Stewart (Institute of Medical Biology, A*STAR) for providing iMEF$^{-/-}$ cells.

Conflict of Interest statement. One of the authors has reported a direct financial conflict of interest: H.J.W. is a member of the Scientific Advisory Board of and owns equity in Allomek Therapeutics, LLC, which is developing a MEK1/2 inhibitor for the treatment of *LMNA* cardiomyopathy.

Funding

Research reported in this publication was supported by the National Heart Lung and Blood Institute of the National Institutes of Health under award number R00HL118163 and the National Institute of Arthritis and Musculoskeletal and Skin Diseases of the National Institutes of Health under award number R01AR04897. The content is solely the responsibility of the authors and does not necessarily represent the official views of the National Institutes of Health.

References

1. Dauer, W.T. and Worman, H.J. (2009) The nuclear envelope as a signaling node in development and disease. *Dev. Cell*, **17**, 626–638.

2. Bonne, G., Di Barletta, M.R., Varnous, S., Becane, H.M., Hammouda, E.H., Merlini, L., Muntoni, F., Greenberg, C.R., Gary, F., Urtizberea, J.A. *et al.* (1999) Mutations in the gene encoding lamin A/C cause autosomal dominant Emery-Dreifuss muscular dystrophy. *Nat. Genet.*, **21**, 285–288.
3. Brodsky, G.L., Muntoni, F., Miocic, S., Sinagra, G., Sewry, C. and Mestroni, L. (2000) Lamin A/C gene mutation associated with dilated cardiomyopathy with variable skeletal muscle involvement. *Circulation*, **101**, 473–476.
4. Fatkin, D., MacRae, C., Sasaki, T., Wolff, M.R., Porcu, M., Frenneaux, M., Atherton, J., Vidaillet, H.J., Jr., Spudich, S., De Girolami, U. *et al.* (1999) Missense mutations in the rod domain of the lamin A/C gene as causes of dilated cardiomyopathy and conduction-system disease. *N. Engl. J. Med.*, **341**, 1715–1724.
5. Muchir, A., van Engelen, B.G., Lammens, M., Mislow, J.M., McNally, E., Schwartz, K. and Bonne, G. (2003) Nuclear envelope alterations in fibroblasts from LGMD1B patients carrying nonsense Y259X heterozygous or homozygous mutation in lamin A/C gene. *Exp. Cell Res.*, **291**, 352–362.
6. Cowan, J., Li, D., Gonzalez-Quintana, J., Morales, A. and Hershberger, R.E. (2010) Morphological analysis of 13 LMNA variants identified in a cohort of 324 unrelated patients with idiopathic or familial dilated cardiomyopathy. *Circ. Cardiovasc. Genet.*, **3**, 6–14.
7. Lu, J.T., Muchir, A., Nagy, P.L. and Worman, H.J. (2011) LMNA cardiomyopathy: cell biology and genetics meet clinical medicine. *Dis. Model. Mech.*, **4**, 562–568.
8. Raman, S.V., Sparks, E.A., Baker, P.M., McCarthy, B. and Wooley, C.F. (2007) Mid-myocardial fibrosis by cardiac magnetic resonance in patients with lamin A/C cardiomyopathy: possible substrate for diastolic dysfunction. *J. Cardiovasc. Magn. Reson.*, **9**, 907–913.
9. Taylor, M.R., Fain, P.R., Sinagra, G., Robinson, M.L., Robertson, A.D., Carniel, E., Di Lenarda, A., Bohlmeyer, T.J., Ferguson, D.A., Brodsky, G.L. *et al.* (2003) Natural history of dilated cardiomyopathy due to lamin A/C gene mutations. *J. Am. Coll. Cardiol.*, **41**, 771–780.
10. van Tintelen, J.P., Hofstra, R.M., Katerberg, H., Rossenbacker, T., Wiesfeld, A.C., du Marchie Sarvaas, G.J., Wilde, A.A., van Langen, I.M., Nannenberg, E.A., van der Kooi, A.J. *et al.* (2007) High yield of LMNA mutations in patients with dilated cardiomyopathy and/or conduction disease referred to cardiogenetics outpatient clinics. *Am. Heart. J.*, **154**, 1130–1139.
11. Vytopil, M., Benedetti, S., Ricci, E., Galluzzi, G., Dello Russo, A., Merlini, L., Boriani, G., Gallina, M., Morandi, L., Politano, L. *et al.* (2003) Mutation analysis of the lamin A/C gene (LMNA) among patients with different cardiomuscular phenotypes. *J. Med. Genet.*, **40**, e132.
12. Turgay, Y., Eibauer, M., Goldman, A.E., Shimi, T., Khayat, M., Ben-Harush, K., Dubrovsky-Gaupp, A., Sapra, K.T., Goldman, R.D. and Medalia, O. (2017) The molecular architecture of lamins in somatic cells. *Nature*, **543**, 261–264.
13. Solovei, I., Wang, A.S., Thanisch, K., Schmidt, C.S., Krebs, S., Zwerger, M., Cohen, T.V., Devys, D., Foisner, R., Peichl, L. *et al.* (2013) LBR and lamin A/C sequentially tether peripheral heterochromatin and inversely regulate differentiation. *Cell*, **152**, 584–598.
14. Oldenburg, A., Briand, N., Sorensen, A.L., Cahyani, I., Shah, A., Moskaug, J.O. and Collas, P. (2017) A lipodystrophy-causing lamin A mutant alters conformation and epigenetic regulation of the anti-adipogenic MIR335 locus. *J. Cell Biol.*, **216**, 2731–2743.
15. Gonzalez, J.M., Navarro-Puche, A., Casar, B., Crespo, P. and Andres, V. (2008) Fast regulation of AP-1 activity through interaction of lamin A/C, ERK1/2, and c-Fos at the nuclear envelope. *J. Cell Biol.*, **183**, 653–666.
16. Rodriguez, J., Calvo, F., Gonzalez, J.M., Casar, B., Andres, V. and Crespo, P. (2010) ERK1/2 MAP kinases promote cell cycle entry by rapid, kinase-independent disruption of retinoblastoma-lamin A complexes. *J. Cell Biol.*, **191**, 967–979.
17. Muchir, A., Pavlidis, P., Decostre, V., Herron, A.J., Arimura, T., Bonne, G. and Worman, H.J. (2007) Activation of MAPK pathways links LMNA mutations to cardiomyopathy in Emery-Dreifuss muscular dystrophy. *J. Clin. Invest.*, **117**, 1282–1293.
18. Muchir, A., Reilly, S.A., Wu, W., Iwata, S., Homma, S., Bonne, G. and Worman, H.J. (2012) Treatment with selumetinib preserves cardiac function and improves survival in cardiomyopathy caused by mutation in the lamin A/C gene. *Cardiovasc. Res.*, **93**, 311–319.
19. Arimura, T., Helbling-Leclerc, A., Massart, C., Varnous, S., Niel, F., Lacene, E., Fromes, Y., Toussaint, M., Mura, A.M., Keller, D.I. *et al.* (2005) Mouse model carrying H222P-Lmna mutation develops muscular dystrophy and dilated cardiomyopathy similar to human striated muscle laminopathies. *Hum. Mol. Genet.*, **14**, 155–169.
20. Wu, W., Muchir, A., Shan, J., Bonne, G. and Worman, H.J. (2011) Mitogen-activated protein kinase inhibitors improve heart function and prevent fibrosis in cardiomyopathy caused by mutation in lamin A/C gene. *Circulation*, **123**, 53–61.
21. Wu, W., Iwata, S., Homma, S., Worman, H.J. and Muchir, A. (2014) Depletion of extracellular signal-regulated kinase 1 in mice with cardiomyopathy caused by lamin A/C gene mutation partially prevents pathology before isoenzyme activation. *Hum. Mol. Genet.*, **23**, 1–11.
22. Wu, W., Chordia, M.D., Hart, B.P., Kumarasinghe, E.S., Ji, M.K., Bhargava, A., Lawlor, M.W., Shin, J.Y., Sera, F., Homma, S. *et al.* (2017) Macrocyclic MEK1/2 inhibitor with efficacy in a mouse model of cardiomyopathy caused by lamin A/C gene mutation. *Bioorg. Med. Chem.*, **25**, 1004–1013.
23. Choi, J.C., Wu, W., Muchir, A., Iwata, S., Homma, S. and Worman, H.J. (2012) Dual specificity phosphatase 4 mediates cardiomyopathy caused by lamin A/C (LMNA) gene mutation. *J. Biol. Chem.*, **287**, 40513–40524.
24. Choi, J.C., Muchir, A., Wu, W., Iwata, S., Homma, S., Morrow, J.P. and Worman, H.J. (2012) Temsirolimus activates autophagy and ameliorates cardiomyopathy caused by lamin A/C gene mutation. *Sci. Transl. Med.*, **4**, 144ra102.
25. Brondello, J.M., Brunet, A., Pouyssegur, J. and McKenzie, F.R. (1997) The dual specificity mitogen-activated protein kinase phosphatase-1 and -2 are induced by the p42/p44MAPK cascade. *J. Biol. Chem.*, **272**, 1368–1376.
26. Guan, K.L. and Butch, E. (1995) Isolation and characterization of a novel dual specific phosphatase, HVH2, which selectively dephosphorylates the mitogen-activated protein kinase. *J. Biol. Chem.*, **270**, 7197–7203.
27. Misra-Press, A., Rim, C.S., Yao, H., Roberson, M.S. and Stork, P.J. (1995) A novel mitogen-activated protein kinase phosphatase. Structure, expression, and regulation. *J. Biol. Chem.*, **270**, 14587–14596.
28. Chu, Y., Solski, P.A., Khosravi-Far, R., Der, C.J. and Kelly, K. (1996) The mitogen-activated protein kinase phosphatases PAC1, MKP-1, and MKP-2 have unique substrate specificities and reduced activity in vivo toward the ERK2 sevenmaker mutation. *J. Biol. Chem.*, **271**, 6497–6501.

29. Hirsch, D.D. and Stork, P.J. (1997) Mitogen-activated protein kinase phosphatases inactivate stress-activated protein kinase pathways in vivo. *J. Biol. Chem.*, **272**, 4568–4575.
30. Robinson, C.J., Sloss, C.M. and Plevin, R. (2001) Inactivation of JNK activity by mitogen-activated protein kinase phosphatase-2 in EAhy926 endothelial cells is dependent upon agonist-specific JNK translocation to the nucleus. *Cell Signal.*, **13**, 29–41.
31. Berasi, S.P., Huard, C., Li, D., Shih, H.H., Sun, Y., Zhong, W., Paulsen, J.E., Brown, E.L., Gimeno, R.E. and Martinez, R.V. (2006) Inhibition of gluconeogenesis through transcriptional activation of EGR1 and DUSP4 by AMP-activated kinase. *J. Biol. Chem.*, **281**, 27167–27177.
32. Carlos, A.R., Escandell, J.M., Kotsantis, P., Suwaki, N., Bouwman, P., Badie, S., Folio, C., Benitez, J., Gomez-Lopez, G., Pisano, D.G. *et al.* (2013) ARF triggers senescence in Brca2-deficient cells by altering the spectrum of p53 transcriptional targets. *Nat. Commun.*, **4**, 2697.
33. Ramesh, S., Qi, X.J., Wildey, G.M., Robinson, J., Molkentin, J., Letterio, J. and Howe, P.H. (2008) TGF beta-mediated BIM expression and apoptosis are regulated through SMAD3-dependent expression of the MAPK phosphatase MKP2. *EMBO Rep.*, **9**, 990–997.
34. Shen, W.H., Wang, J., Wu, J., Zhurkin, V.B. and Yin, Y. (2006) Mitogen-activated protein kinase phosphatase 2: a novel transcription target of p53 in apoptosis. *Cancer Res.*, **66**, 6033–6039.
35. Wang, J., Shen, W.H., Jin, Y.J., Brandt-Rauf, P.W. and Yin, Y. (2007) A molecular link between E2F-1 and the MAPK cascade. *J. Biol. Chem.*, **282**, 18521–18531.
36. Zhang, T., Choy, M., Jo, M. and Roberson, M.S. (2001) Structural organization of the rat mitogen-activated protein kinase phosphatase 2 gene. *Gene*, **273**, 71–79.
37. Zhang, T., Wolfe, M.W. and Roberson, M.S. (2001) An early growth response protein (Egr) 1 cis-element is required for gonadotropin-releasing hormone-induced mitogen-activated protein kinase phosphatase 2 gene expression. *J. Biol. Chem.*, **276**, 45604–45613.
38. Hsiao, W.Y., Lin, Y.C., Liao, F.H., Chan, Y.C. and Huang, C.Y. (2015) Dual-specificity phosphatase 4 regulates STAT5 protein stability and helper T cell polarization. *PLoS One*, **10**, e0145880.
39. Jeong, M.W., Kang, T.H., Kim, W., Choi, Y.H. and Kim, K.T. (2013) Mitogen-activated protein kinase phosphatase 2 regulates histone H3 phosphorylation via interaction with vaccinia-related kinase 1. *Mol. Biol. Cell*, **24**, 373–384.
40. Eghbali, M., Blumenfeld, O.O., Seifter, S., Buttrick, P.M., Leinwand, L.A., Robinson, T.F., Zern, M.A. and Giambrone, M.A. (1989) Localization of types I, III and IV collagen mRNAs in rat heart cells by in situ hybridization. *J. Mol. Cell. Cardiol.*, **21**, 103–113.
41. Eghbali, M., Czaja, M.J., Zeydel, M., Weiner, F.R., Zern, M.A., Seifter, S. and Blumenfeld, O.O. (1988) Collagen chain mRNAs in isolated heart cells from young and adult rats. *J. Mol. Cell. Cardiol.*, **20**, 267–276.
42. Shumaker, D.K., Dechat, T., Kohlmaier, A., Adam, S.A., Bozovsky, M.R., Erdos, M.R., Eriksson, M., Goldman, A.E., Khuon, S., Collins, F.S. *et al.* (2006) Mutant nuclear lamin A leads to progressive alterations of epigenetic control in premature aging. *Proc. Natl. Acad. Sci. U. S. A.*, **103**, 8703–8708.
43. Chatzifrangkeskou, M., Le Dour, C., Wu, W., Morrow, J.P., Joseph, L.C., Beuvin, M., Sera, F., Homma, S., Vignier, N., Mougenot, N. *et al.* (2016) ERK1/2 directly acts on CTGF/CCN2 expression to mediate myocardial fibrosis in cardiomyopathy caused by mutations in the lamin A/C gene. *Hum. Mol. Genet.*, **25**, 2220–2233.
44. Auger-Messier, M., Accornero, F., Goonasekera, S.A., Bueno, O.F., Lorenz, J.N., van Berlo, J.H., Willette, R.N. and Molkentin, J.D. (2013) Unrestrained p38 MAPK activation in Dusp1/4 double-null mice induces cardiomyopathy. *Circ. Res.*, **112**, 48–56.
45. Kroemer, G., Marino, G. and Levine, B. (2010) Autophagy and the integrated stress response. *Mol. Cell*, **40**, 280–293.
46. Yang, Z. and Klionsky, D.J. (2010) Mammalian autophagy: core molecular machinery and signaling regulation. *Curr. Opin. Cell Biol.*, **22**, 124–131.
47. Arimura, T., Onoue, K., Takahashi-Tanaka, Y., Ishikawa, T., Kuwahara, M., Setou, M., Shigenobu, S., Yamaguchi, K., Bertrand, A.T., Machida, N. *et al.* (2013) Nuclear accumulation of androgen receptor in gender difference of dilated cardiomyopathy due to lamin A/C mutations. *Cardiovasc. Res.*, **99**, 382–394.
48. Altamirano, F., Oyarce, C., Silva, P., Toyos, M., Wilson, C., Lavandero, S., Uhlen, P. and Estrada, M. (2009) Testosterone induces cardiomyocyte hypertrophy through mammalian target of rapamycin complex 1 pathway. *J. Endocrinol.*, **202**, 299–307.
49. Kumar, S., Baldinger, S.H., Gandjbakhch, E., Maury, P., Sellal, J.M., Androulakis, A.F., Waintraub, X., Charron, P., Rollin, A., Richard, P. *et al.* (2016) Long-term arrhythmic and nonarrhythmic outcomes of lamin A/C mutation carriers. *J. Am. Coll. Cardiol.*, **68**, 2299–2307.
50. van Rijsingen, I.A., Nannenberg, E.A., Arbustini, E., Elliott, P.M., Mogensen, J., Hermans-van Ast, J.F., van der Kooi, A.J., van Tintelen, J.P., van den Berg, M.P., Grasso, M. *et al.* (2013) Gender-specific differences in major cardiac events and mortality in lamin A/C mutation carriers. *Eur. J. Heart Fail.*, **15**, 376–384.
51. Adams, K.F., Jr., Dunlap, S.H., Sueta, C.A., Clarke, S.W., Patterson, J.H., Blauwet, M.B., Jensen, L.R., Tomasko, L. and Koch, G. (1996) Relation between gender, etiology and survival in patients with symptomatic heart failure. *J. Am. Coll. Cardiol.*, **28**, 1781–1788.
52. O'Meara, E., Clayton, T., McEntegart, M.B., McMurray, J.J., Pina, I.L., Granger, C.B., Ostergren, J., Michelson, E.L., Solomon, S.D., Pocock, S. *et al.* (2007) Sex differences in clinical characteristics and prognosis in a broad spectrum of patients with heart failure: results of the Candesartan in Heart failure: assessment of Reduction in Mortality and morbidity (CHARM) program. *Circulation*, **115**, 3111–3120.
53. Muchir, A., Kim, Y.J., Reilly, S.A., Wu, W., Choi, J.C. and Worman, H.J. (2013) Inhibition of extracellular signal-regulated kinase 1/2 signaling has beneficial effects on skeletal muscle in a mouse model of Emery-Dreifuss muscular dystrophy caused by lamin A/C gene mutation. *Skelet. Muscle*, **3**, 17.
54. Sullivan, T., Escalante-Alcalde, D., Bhatt, H., Anver, M., Bhat, N., Nagashima, K., Stewart, C.L. and Burke, B. (1999) Loss of A-type lamin expression compromises nuclear envelope integrity leading to muscular dystrophy. *J. Cell Biol.*, **147**, 913–920.
55. Ivorra, C., Kubicek, M., Gonzalez, J.M., Sanz-Gonzalez, S.M., Alvarez-Barrientos, A., O'Connor, J.E., Burke, B. and Andres, V. (2006) A mechanism of AP-1 suppression through interaction of c-Fos with lamin A/C. *Genes Dev.*, **20**, 307–320.
56. Cagnol, S. and Rivard, N. (2013) Oncogenic KRAS and BRAF activation of the MEK/ERK signaling pathway promotes

expression of dual-specificity phosphatase 4 (DUSP4/MKP2) resulting in nuclear ERK1/2 inhibition. *Oncogene*, **32**, 564–576.
57. Crowell, S., Wancket, L.M., Shakibi, Y., Xu, P., Xue, J., Samavati, L., Nelin, L.D. and Liu, Y. (2014) Post-translational regulation of mitogen-activated protein kinase phosphatase (MKP)-1 and MKP-2 in macrophages following lipopolysaccharide stimulation: the role of the C termini of the phosphatases in determining their stability. *J. Biol. Chem.*, **289**, 28753–28764.
58. Ramos, F.J., Chen, S.C., Garelick, M.G., Dai, D.F., Liao, C.Y., Schreiber, K.H., MacKay, V.L., An, E.H., Strong, R., Ladiges, W.C. *et al.* (2012) Rapamycin reverses elevated mTORC1 signaling in lamin A/C-deficient mice, rescues cardiac and skeletal muscle function, and extends survival. *Sci. Transl. Med.*, **4**, 144ra103.
59. Inoki, K., Corradetti, M.N. and Guan, K.L. (2005) Dysregulation of the TSC-mTOR pathway in human disease. *Nat. Genet.*, **37**, 19–24.
60. Inoki, K., Li, Y., Xu, T. and Guan, K.L. (2003) Rheb GTPase is a direct target of TSC2 GAP activity and regulates mTOR signaling. *Genes Dev.*, **17**, 1829–1834.
61. Inoki, K., Li, Y., Zhu, T., Wu, J. and Guan, K.L. (2002) TSC2 is phosphorylated and inhibited by Akt and suppresses mTOR signalling. *Nat. Cell Biol.*, **4**, 648–657.
62. Long, X., Lin, Y., Ortiz-Vega, S., Yonezawa, K. and Avruch, J. (2005) Rheb binds and regulates the mTOR kinase. *Curr. Biol.*, **15**, 702–713.
63. Jung, C.H., Jun, C.B., Ro, S.H., Kim, Y.M., Otto, N.M., Cao, J., Kundu, M. and Kim, D.H. (2009) ULK-Atg13-FIP200 complexes mediate mTOR signaling to the autophagy machinery. *Mol. Biol. Cell*, **20**, 1992–2003.
64. Ma, L., Chen, Z., Erdjument-Bromage, H., Tempst, P. and Pandolfi, P.P. (2005) Phosphorylation and functional inactivation of TSC2 by Erk implications for tuberous sclerosis and cancer pathogenesis. *Cell*, **121**, 179–193.
65. Vega, R.B., Konhilas, J.P., Kelly, D.P. and Leinwand, L.A. (2017) Molecular mechanisms underlying cardiac adaptation to exercise. *Cell Metab.*, **25**, 1012–1026.
66. Shiojima, I., Sato, K., Izumiya, Y., Schiekofer, S., Ito, M., Liao, R., Colucci, W.S. and Walsh, K. (2005) Disruption of coordinated cardiac hypertrophy and angiogenesis contributes to the transition to heart failure. *J. Clin. Invest.*, **115**, 2108–2118.
67. Shiojima, I., Schiekofer, S., Schneider, J.G., Belisle, K., Sato, K., Andrassy, M., Galasso, G. and Walsh, K. (2012) Short-term akt activation in cardiac muscle cells improves contractile function in failing hearts. *Am. J. Pathol.*, **181**, 1969–1976.
68. Jeffrey, K.L., Camps, M., Rommel, C. and Mackay, C.R. (2007) Targeting dual-specificity phosphatases: manipulating MAP kinase signalling and immune responses. *Nat. Rev. Drug Discov.*, **6**, 391–403.
69. Jeong, D.G., Jung, S.K., Yoon, T.S., Woo, E.J., Kim, J.H., Park, B.C., Ryu, S.E. and Kim, S.J. (2009) Crystal structure of the catalytic domain of human MKP-2 reveals a 24-mer assembly. *Proteins*, **76**, 763–767.
70. Muchir, A., Shan, J., Bonne, G., Lehnart, S.E. and Worman, H.J. (2008) Inhibition of extracellular signal-regulated kinase signaling to prevent cardiomyopathy caused by mutation in the gene encoding A-type lamins. *Hum. Mol. Genet.*, **18**, 241–247.
71. Al-Mutairi, M.S., Cadalbert, L.C., McGachy, H.A., Shweash, M., Schroeder, J., Kurnik, M., Sloss, C.M., Bryant, C.E., Alexander, J. and Plevin, R. (2010) MAP kinase phosphatase-2 plays a critical role in response to infection by Leishmania mexicana. *PLoS Pathog.*, **6**, e1001192.
72. Pages, G., Guerin, S., Grall, D., Bonino, F., Smith, A., Anjuere, F., Auberger, P. and Pouyssegur, J. (1999) Defective thymocyte maturation in p44 MAP kinase (Erk 1) knockout mice. *Science*, **286**, 1374–1377.
73. Jahn, D., Schramm, S., Schnolzer, M., Heilmann, C.J., de Koster, C.G., Schutz, W., Benavente, R. and Alsheimer, M. (2012) A truncated lamin A in the Lmna -/- mouse line: implications for the understanding of laminopathies. *Nucleus*, **3**, 463–474.
74. Mauro, C., Leow, S.C., Anso, E., Rocha, S., Thotakura, A.K., Tornatore, L., Moretti, M., De Smaele, E., Beg, A.A., Tergaonkar, V. *et al.* (2011) NF-kappaB controls energy homeostasis and metabolic adaptation by upregulating mitochondrial respiration. *Nat. Cell Biol.*, **13**, 1272–1279.
75. Livak, K.J. and Schmittgen, T.D. (2001) Analysis of relative gene expression data using real-time quantitative PCR and the 2(-Delta Delta C(T)) Method. *Methods*, **25**, 402–408.
76. Abramoff, M.D., Magalhaes, P.J. and Ram, S.J. (2004) Image processing with ImageJ. *Biophotonics Int.*, **11**, 36–42.
77. Weinmann, A.S. and Farnham, P.J. (2002) Identification of unknown target genes of human transcription factors using chromatin immunoprecipitation. *Methods*, **26**, 37–47.
78. Bolte, S. and Cordelieres, F.P. (2006) A guided tour into subcellular colocalization analysis in light microscopy. *J. Microsc.*, **224**, 213–232.
79. Laemmli, U.K. (1970) Cleavage of structural proteins during the assembly of the head of bacteriophage T4. *Nature*, **227**, 680–685.